PROCESSING AND CHARACTERIZATION OF NEMATIC CO-POLYMER PHBA/PET NANOCOMPOSITE FILMS VIA HOT-MELT EXTRUSION

by

Félix G. Miranda Mendoza

A thesis submitted in partial fulfillment of the requirements for the degree of

MASTER IN SCIENCE

in

CHEMICAL ENGINEERING

UNIVERSITY OF PUERTO RICO

MAYAGÜEZ CAMPUS

2011

Approved by:

Aldo Acevedo, PhD President, Graduate Committee	Date
Julio Briano, PhD Member, Graduate Committee	Date
Maria M. Martínez Iñesta, PhD Member, Graduate Committee	Date
Ubaldo Cordova, PhD Member, Graduate Committee	Date
O. Marcelo Suarez, PhD Graduate Studies Representative	Date
Aldo Acevedo, PhD Acting Chairperson of the Department	Date

ABSTRACT

In this research work, the effect of particle shape (i.e. rod-like, spherical and platellet) and concentration on the liquid crystalline structure of poly (4-benzoic acid-co-ethylene terephthalate) (PHBA/PET) was evaluated by studying the composites thermal transitions and structure. Composite films were produced by direct melt blending of the polymer with up to 1.5 v% loadings of four different kinds of commercial fillers, which are: silica, multiwalled carbon nanotubes (MWCNT), halloysite nanoclays (HNC) and montmorillonite nanoclays (MNC). Mixture and processing was carried out in a Thermo-Haake MiniLab2 twin-screw extruder. Thermal transitions were determined by differential scanning calorimetry (DSC), thermogravimetric analysis (TGA) and polarized optical microscopy (POM). Structure and morphology were analyzed by a combination of small angle X-ray scattering (SAXS), and scanning electron microscopy (SEM).

No significant changes were observed on the glass and melting transitions since all the values are within the experimental error independent of particle type. An exception was the melting of MNC composites since from medium to high values (0.5 v%-1.5 v %) the melting temperature decreased but remained independent of particle loading. The isotropic-to-nematic transition temperature was diminished with the addition of particles for all cases, but was independent of concentration. This represented a decrease in the liquid crystalline region.

Thermal degradation was also studied by 5 and 10 % of weight loss and at the maximum rate of degradation. All particles showed to produce a positive increment in

composite thermal stability, except for MWCNT where temperatures remained almost constant. This behavior could be explained by the molecular confinement due to the increment in particle concentration of the MWCNT in PET rich region.

The highly anisotropic nanoparticles (i.e. rods & plates) had a similar effect on the morphology, showing a fibrilar behavior at the fracture plane, as observed by the SEM, while silica showed no fibrillar structures. This was attributed to the non-preferential arrangement of the silica spheres. No significant changes were observed on the SAXS patterns for HNC or MWCNT, while silica and MNC composites showed a slightly wider SAXS pattern. The latter can be attributed to the presence of a broader domain distribution.

Addition of this kind of nanoparticles at the low concentrations studied did not showed any significant effect on the LC polymer thermal transitions. Also, no change is observed on the liquid crystalline structure for the rod-like particles while silica and clay particles promote large crystal domains distributions as evidenced by SAXS. In the case of thermal stability it seems that particles intrinsic properties are the factor that promotes the enhancement on temperature resistance rather than their shape or concentration.

RESUMEN

En este trabajo investigativo se estudió el efecto que tiene la adición de nanoparticulas con diferente morfología (i.e. cilíndricas, esféricas y hojuela) al igual que la concentración, en la naturaleza liquido cristalina del polímero poly(4-hydroxy-benzoic acid-co-ethylene terephtalate) (PHBA/PET). Esto se hizo mediante el estudio de las transiciones termales y la estructura interna del compuesto. Las tiras de nanocompuestos fueron procesadas mediante la mezcla directa la matriz con cuatro diferentes tipos de nanoparticulas comerciales, las cuales son: silica, nanotubos de carbón de multiples paredes (MWCNT), halloysite nanoclays (HNC) y montmorillonite nanoclay (MNC). La mezcla y el procesamiento se llevó a cabo en una extrusora de doble barrena Thermo-Haake MiniLab2 con concentraciones hasta 1.5 v%. Las transiciones termales se determinaron a través del uso de un dispositivo de rastreo diferencial de calor o DSC, por sus siglas en inglés, mientras que la durabilidad o resistencia termal se estudió usando un analizador termogravimetrico o TGA y mediante microscopia óptica polarizada (POM). La estructura y morfología de los compuestos se analizaron utilizando el análisis de rayos X a ángulos pequeños y dispersos (SAXS) al igual que el microscopio de rastreo electrónico (SEM).

No se observaron cambios significativos en las transiciones vítreas y de fusión dado que todos los valores se mantuvieron dentro del error experimental independientemente del tipo de morfología de la partícula. A excepción de la temperatura de fusión para el sistema con MNC ya que de valores medianos a altos en concentración (0.5 v%-1.5 v%) el valor de la temperatura para esta transición disminuyo para todos los casos pero independiente de concentración. Este comportamiento se reflejó como una disminución en la zona liquido cristalina.

La degradación termal fue estudiada a 5 y 10% de pérdida de peso y a las temperaturas de mayor razón de degradación. Todas las partículas mostraron el tener un efecto de aumentar la estabilidad termal de los compuestos a excepción de los MWCNT, donde las temperaturas permanecieron relativamente constantes. Este comportamiento se puede explicar debido al confinamiento molecular provocado por el aumento en concentración de MWCNT en las regiones ricas en PET.

Las nanoparticulas altamente anisotropicas (i.e. cilindros y hojuelas) provocan un efecto similar en la morfología, mostrando un comportamiento fibrilar en el plano de fractura, como se observa en el SEM; mientras que silica demostró no promover el comportamiento fibrilar. Esto se le atribuye al arreglo no preferencial que tienen las esferas de silica. Tampoco se observaron cambios significativos en las curvas de SAXS.

La adición de este tipo de nanoparticulas, a las bajas concentraciones estudiadas, no demostró tener un efecto significativo en las transiciones termales del cristal líquido. Tampoco se observó cambio alguno en la estructura liquido cristalina para las partículas con morfología cilíndrica, mientras que silica y los clays promovieron la formación de zonas o dominios de cristales distribuidos. En el caso de la estabilidad termal, al parecer el factor que influye grandemente son las propiedades intrínsecas de cada partícula y no la morfología o concentración de las mismas, esto para las concentraciones estudiadas.

ACKNOWLEDGMENTS

I would like to thank my advisor, Prof. Aldo Acevedo, for guiding me all these years, including my undergraduate research. I thank him for giving me the opportunity to be part of his research team and his patience. Having been here has given me the opportunity to live many experiences that have helped me grow, both personally and professionally. I also want to thank my laboratory mates for their help and support. Similarly, although without mentioning names, in this journey there have been some people who have helped me in so many ways and I appreciate their friendship, and thank them. Above all, I thank God and my family, since they are everything to me and my reason for being.

I also want to thank the National Science Foundation, the Chemical Engineering Department, and $Wi(PR)_2EM$ for their financial support.

TABLE OF CONTENTS

LIST OF TABLES

LIST OF FIGURES

1. INTRODUCTION

The study of polymer composites has increased markedly in the last few years due to the necessity of materials and structures with enhanced and multifunctional properties, yet maintaining processing ease and lower costs. The selection of an efficient matrix and filler is determined by design and application requirements. The size of fillers has been typically on the micrometer scale, but recently the interest has turned to the nanometer scale. Nanoparticles have attracted the attention as polymer fillers due to their capacity to provide a high surface area per unit volume for physical and chemical processes to occur. Thus, large enhancements in physical properties, such as thermal, mechanical and electrical properties, may be attained with lower amounts of particles [1, 2]. Nevertheless, the addition of nanoparticles could also result in detrimental effects to the matrix, especially if it has internal structure such as the inherent ordering of liquid crystals. As a consequence, polymer nanocomposite production is an optimization problem between formulation composition and internal structure, where enhancements are desired without affecting the performance of the matrix.

A group of specialty polymers known as liquid crystalline polymers (LCPs) are attractive candidates for nanocomposites since they are anisotropic, which means they have positional and/or orientational order. As a result, they have a relatively high degree of molecular orientation, mechanical strength, and resistance to different hostile environments, such as humid, high temperature, or chemically challenging systems. These properties make LCPs attractive in industrial applications such as automobile, aircraft, military, electronics and biomedical applications [3, 4]. Polymer melts in the

nematic liquid crystalline phase, where only orientational order exists, have a great advantage over other kinds of polymers since they have lower viscosities at high shear rates which make them easier to process. On the other hand, the internal anisotropy of the nematic phase has the potential to orient the nanoparticles, since the particle's size is of the same length-scale as that of the polymer molecules. Also the high shearing forces present during processing may orient the particles and LCP molecules along the flow direction, thus obtaining unidirectional LCP nanocomposites.

The goal of this research work is to ***determine the effect of material formulation on the physical properties of model liquid crystalline polymer – based nanocomposite melts and extruded films.*** In order to achieve this objective the effect of particle shape (or equivalently anisotropy) and concentration on the physical properties as well as on the LCP structure are going to be studied. This also requires the optimization of processing conditions to enhance the dispersion of particles within the liquid crystalline polymer matrix.

2. BACKGROUND

2.1 Composites and Polymer Nanocomposites

The concept of composites is not a human invention; it already exists in nature. Typical examples of composites found in nature are ourselves, been the skin and tissues the matrix and the bones our reinforcements. The bones are also classified as natural composites that consist of an organic component called collagen (a fibrous protein) with small amounts of protein, polysaccharides and glycoaminoglycans [5]. Another example is wood who is a composite of cellulose fibers in a matrix of lignin. Also invertebrate shells are composites which are stronger and tougher than some man-made advanced composites [6]. In some countries people have taken advantage of composites by centuries mixing husk or straws with clays to build houses.

The traditional approach to the development of composites is to manipulate some properties in order to enhance predetermined functional requirements which are guided by design necessities. Recently, however, there has been an increasing interest in the development of materials and structures which have value-added properties that can be resumed as mechanical and non-mechanical. Examples of mechanical properties to be enhanced are: stiffness, strength, fracture toughness and ductility among others. While non-mechanical properties are referred to thermal, electrical and diffusive.

Ultimately a lot of studies have been performed using polymers as the matrix for the production of nanocomposites as engineering materials where mechanical improvements of great relevance have been reported. An example is that the use of

polymers has exceeded the use of steel on a volume basis [7]. Some of the reasons that make them suitable for a wide range of applications are due to their lightweight and relative ease of processing. They are used for automobile parts, aerospace components and consumer goods. Another advantage for the use of polymers as nanocomposite matrices is that they are relatively easy to mold, polymers (plastics) can provide high surface finish area and therefore eliminate several machining operations [8].

It is important to address that nanocomposites are materials that result from mixing a matrix (bulk) with one or more nanoparticles. The product obtained has properties of both, the matrix and filler phases that form the nanocomposites [9]. This is due to the interaction of the nanoparticles with the matrix which can result in an enhancement of the matrix properties. For example, Koartar and colleagues [10] reported an increase of 1000% on the loss modulus of polycarbonate (PC) without significant reductions in the storage modulus when PC was loaded with 2 wt% of single-walled carbon nanotubes (SWCNT's). This was attributed to the frictional sliding at the interface between the SWCNT's and the PC molecules. Other example where nanoparticles improved polymer properties was the study reported by Uddin and Sun [11] where the addition of silica nanoparticles to an unidirectional E-glass/epoxy composite resulted in a significant enhancement of the longitudinal compressive strength and modulus.

There are three different types of nanocomposites depending on the length scales of the dispersed particles that are in the order of nanometers. When the three length scales are in the order of nanometers the nanoparticles are known as iso-dimensional or one-dimensional, such as spherical silica nanoparticles. The second is

when two dimensions are in the nanometer scale and a third is larger (usually in micrometers) which forms an elongated structure such as nanotubes. The third type is when just one of the lengths is nanometric, such as lamellar clays [12]. Nanocomposites can also be divided, based on their dispersion in the host matrix, into the following types: phase separated, exfoliated and intercalated. Figure 1 shows the schematic representation for a lamellar nanocomposite. Usually polymers are used as matrix for composite production due to its functional chemical properties; intercalated structures can be defined as the alternation of polymer chains with the particle layers in a fixed compositional ratio and have a well-defined number of polymer layers in the intralamellar space. While exfoliated or delaminated structures are those which the number of polymer chains between the layers is almost continuously variable [13].

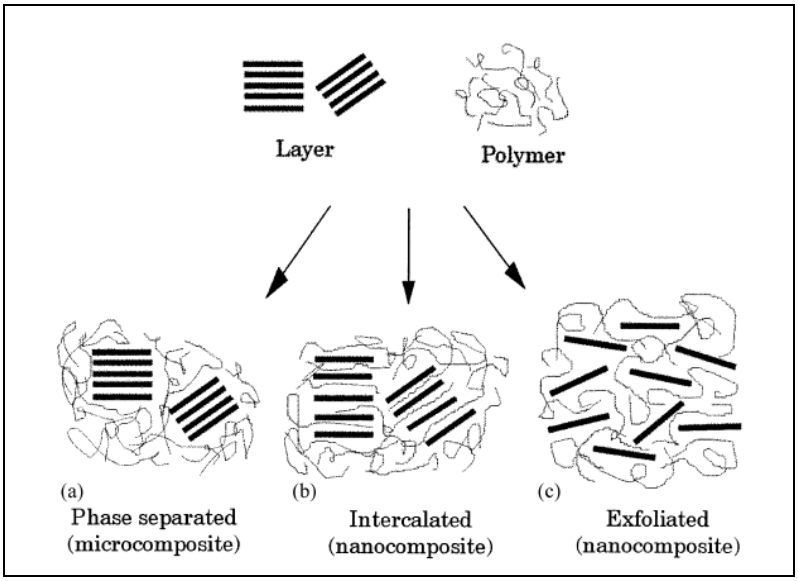

Figure 2.1 Schematic of dispersed lamellar nanoparticles in a polymer matrix. Reproduced from reference [8].

Researchers have become more interested in studying polymer nanocomposites because they have exceptional properties [14]. Some studies have shown that the addition of small amounts of nanoparticles such as carbon nanotubes (CNT's) in polymer matrices may improve their applications in the fields of reinforcing nanocomposites, electronic devices, fire retardants, and many more, as Campell and Shen demonstrates [15, 16]. But it is important to address that the value of nanocomposite technology is not based solely on mechanical enhancements of the neat resin or matrix. Rather, its value comes from providing the so called value-added properties without sacrificing the inherent processability and minimizing detrimental effects on the other properties of the matrix [8].

Polymer nanocomposites also have a broad field of applications in various consumer products, and in the construction and transportation industry, with specific impact on technologies like drink packaging applications, protective coatings, adhesive molding and barrier layer materials. An example of an application improvement in bottling is the use of polymers like PET with nanoclays to produce a nanocomposite of low permeability which will protect the beverages from losing gaseous components [17, 18]. Another example of non-mechanical property enhancement in polymer nanocomposite are those of Gilman and Herrera-Alonso [19-21] and their respective colleagues who have demonstrated the flame retardancy and barrier properties of many polymer/clay nanocomposites like nylon-6 clay nanocomposites. Nanocomposites also have an impact in optical applications like optical data communication and storage, optical sensors and UV protection, such as polycarbonate/alumina and PET/TiO_2 nanocomposites [22, 23]. On the other hand, it also has been demonstrated that some nanoparticles decrease the optical properties in nanocomposites by turning them opaque.

The selection of nanoparticles as matrix reinforcements plays an important role in the composite design since it will determine the composite performance. Particle-matrix interaction is fundamental at the interface because it will determine particle dispersion, property enhancement and as a result, composite reliability. The importance of a good interface between particle and matrix is because it acts as a bridge in the transfer of load and energy from the matrix to the fiber. This is why some researchers propose a surface treatment on the particle before mixing it with the polymer, while others suggest a particle selection with high matrix affinity [24].

There are different forms of reinforcements, from long continuous fibers to woven and short or discontinuous as shown in Figure 2. Each configuration results in an impact of different properties, even if they are of the same material. As mentioned before, it depends on the application, manufacturing method and the properties that have to be enhanced. Typically for the enhancements of mechanical properties long or continuous fibers are recommended while for non-mechanical applications discontinuous fibers are suggested. Thus, great enhancements in mechanical properties are also observed with the use of discontinuous fibers. For the production of short fiber nanocomposites the most common methods used are extrusion, injection and compression molding and for continuous fiber composite filament winding, pultrusion, and roll wrapping are typically used.

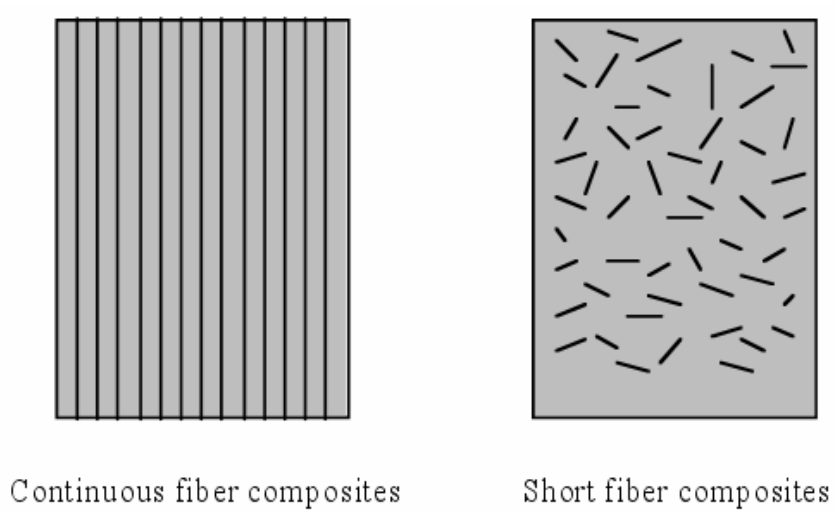

Figure 2.2 Schematic of matrix fillers types.
Reproduced from reference [25].

The reason why long fibers are recommended for structural applications is because the transmitted stress has a continuous path along the fiber axis. While for discontinuous fibers, their high surface area makes them suitable for providing thermal or electrical percolation. It is important to point out that not because the fibers are the reinforcements it means that they are the only ones supporting the systems. Fibers are of little use if the matrix is not present. Some of the important functions of the matrix are: to bind and hold the fibers together, transfer the load to the fiber, provide rigidity and shape to the structure, isolate the fibers so that individual fibers act separately which could stop or slow crack propagation, to provide protection to the fibers from chemical deterioration and mechanical damage and to make the material processable [6].

Until now the advantages of composite material with a special emphasis in polymer nanocomposites have been discussed, but it is necessary also to mention their disadvantages. The most outstanding disadvantage is the very high cost when compared with steel and aluminum. For example, based on weight, the cost of composite materials is 5 to 20 times higher than other engineering materials, such as steel and aluminum, as shown in Table 1.

Table 1.1 Composites and reinforcement costs

Material	Cost [$/lb] *
Glass fiber	1.00 – 8.00
Carbon fiber	8.00 – 40.00
Epoxy	1.50
Glass/epoxy prepreg	12.00
Carbon/epoxy prepreg	12.00 – 60.00
Steel	0.20 – 1.00
Aluminum	0.60 – 1.00

*Costs are based on 2005 prices

Reproduced from reference [6].

.

There is also a deficiency for high volume manufacturing processes. Another disadvantage is that polymers have lower temperature resistance compared with other materials used as matrices (i.e. metals and ceramics) and some of them also have low resistance to solvents and environmental stress cracking. Moisture absorption is also a problem that affects the properties and dimensional stability of composites.

However, the mentioned disadvantages of polymer matrices, there have been an increasing tendency on the use of liquid crystalline polymers for composite production due to their anisotropy and advantageous properties (i.e. processing costs, light weight, endurance). Some properties and advantages of liquid crystalline polymers are discussed in more detail in the next section.

2.2 Liquid crystals and polymers

2.2.1 Introduction to liquid crystals

Liquid crystal (LC) phase is defined as a transition state between the solid and liquid states present in some materials. This phase transition is a thermodynamic stable phase distinguished by the anisotropy of properties in the absence of a three dimensional crystal lattice [26]. The molecules in a liquid crystal may flow like a liquid, but will also have an average orientational and/or positional order as in a solid or crystal-like structure. Liquid crystals may be divided depending on how they are formed, which are thermotropic or lyotropic. Thermotropic liquid crystals are identified as those showing its phases with temperature changes, while lyotropic liquid crystals do so with changes in concentration and need the presence of a solvent [27].

Since the discovery of liquid crystal phases, made by Reinitzer-Lehmann more than 100 years ago, the number of phases in liquid crystals has increased from two (nematic and smectic) to fifteen or twenty. But the most common is the nematic phase, which is characterized for having orientational order, but little or no positional order. The molecular orientation (locally or on average) is denoted by a unit vector **n** called the director. The degree of orientation is given by the order parameter S as:

$$S = \frac{\left\langle 3\cos^2\theta - 1 \right\rangle}{2} \qquad \text{Eqn. 1}$$

The brackets represent the average of all molecules and θ is the angle between every molecule and the director. The value of S ranges from zero to one, being zero the isotropic state and one an ideal orientation where all the molecules are parallel to each other.

Liquid crystals can be also grouped in several types depending on the geometrical structure of the mesogenic molecules. The liquid crystals derived from the rod-shape molecules (i.e., one axis much longer than the others) are called calamitics. These classes of materials are commonly studied and extremely useful for practical applications (e.g., nematic polymer melts). The mesophases formed by disc-like molecules (i.e., one axis shorter than the other two) are called discotics [28]. Also, there are some studies on bent core molecules (i.e., bow-loke or banana shaped) [29-31], but their particular use is limited.

Calamitic thermotropic liquid crystals are mainly subdivided into nematic and smectic mesophases [32]. The smectic mesophase is also divided in several different types of phases, such as S_A, S_B, S_C, …, S_I, which are differentiated by the preferred directional orientation of the molecules with respect to the layer normal and the

distribution of the molecules centers of mass within each layer. In the other hand, the disc-like molecules are subdivided as discotic nematic and columnar [33].

2.2.2 Liquid crystal polymers

The birth of liquid crystalline polymers is attributed to the German chemist Daniel Vorländer when in 1923 he began to pursue the concept of a main-chain liquid crystal polymer. Vorländer studied the systematic increase of benzene rings in rod-like molecules and found that the melting temperature was way above the decomposition temperature, which basically frustrated his study [34, 35]. It was later determined that this happened because the melting point of rigid chain polymers increases rapidly with increasing chain length. It was not until 1970, when Jackson and coworkers in Eastman Kodak were able to synthesize rigid random copolymers of aromatic polyesters [36].

Liquid crystal polymers (LCP's) are divided according to the location of the mesogenic group, which in liquid crystals refers to the semirigid or rigid units attached to the backbone [37]. There are three kinds of liquid crystal polymers (Figure 3a and 3b, which are: (a) main chain liquid crystal polymers, (a) side chain liquid crystal polymers and (c) a combination of both called combined liquid crystal polymers [33].

Rigid main chain liquid crystal polymers can be formed when low molar mass (rod or disc-shaped) mesogenic molecules are joined. While if the linking units are long and flexible a semiflexible polymer is derived. The mesomorphic properties or structural attributes of the LC phase in main chain liquid crystal polymers are strongly influenced by the degree of flexibility and structural composition. In side chain liquid crystal polymers, the flexible polymer backbone has a strong tendency to adopt a random coiled conformation while the attached mesogenic units tend to adopt an anisotropic arrangement.

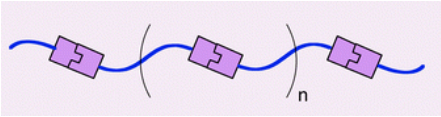

(a) Main chain polymer

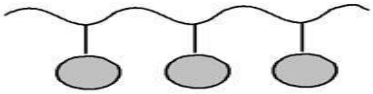

(b) Side chain polymer

Figure 2.3 Schematic mesogenic gropup locations.
Reproduced from reference [38].

2.2.3 Thermotropic liquid crystal polymers

Liquid crystalline polymer melts are widely used for different applications, this kind of polymers are often called thermotropic liquid crystals. Some applications examples are in electronics and high precision mouldings, lightweight aircrafts and, automobile parts, solar cells and many other domestic appliances [37, 39]. It can be said that thermotropic liquid crystalline polymers (TLC) are established as specialty materials, where the polymer manufacturers offer their own variations. As mentioned before, thermotropic liquid crystals show their phases at a certain temperature range. At lower temperatures the material will have a crystal-like behavior while at relatively high temperatures the molecules will flow freely forming an isotropic phase due to the destruction of the cooperative order by thermal motions. It is important to remind that the liquid crystal phenomenon is a thermodynamically stable phase that generally lies between the solid and the isotropic liquid phase and is commonly named mesophase.

The interest in synthesizing thermotropic polymers began with the pursuit of polymers with higher mechanical properties and heat and fire resistance. With this in mind, Economy and coworkers came out with the production of a high molecular weight polymer named poly(4-hydroxybenzoic acid) [40]. But there was a problem of processability due to its high crystallinity and melting point which was around 600°C. In order to lower the melting temperature of the thermotropic polymers, researchers

such as Economy and Jackson started to study the effect of copolymerization on different monomers. From these studies, it was concluded that random copolymerization is an effective way of disturbing the regular molecular structure of the polymer chain and tends to lower the melting temperature [41]. This is due to the lack of repeating monomers of the same molecule which inhibits crystallization and, thus, results in a reduction of the melting temperature. Common examples of thermotropic polymers and copolymers are: polybenzamide (PBA), poly(phenyleneterephthalamide) [26] or Kevlar [42], polybenzobisthiazole (PBT) [43], 4,4'- biphenol, p-hydroxy benzoic acid and terephthalic acid (BPTA/HBA; Ekkcel I-2000) also known as Xydar [44], and poly(4-hydroxy benzoic acid-co-ethylene terephthalate) (PHBA/PET) [45], among others.

The most prominent advantage of thermotropic liquid crystalline polymers is that, under the right processing conditions, they tend to align its molecules and remain in that orientation [46]. This advantageous behavior is due to the fibrous nature of LCP's which makes them self – reinforcing polymers and as a result translates into better mechanical properties. It has been found that TLCP/TLCP blends have better characteristics than those of individual TLCP [47-51]. A typical example of improvement is the ability of lowering the viscosity in order to make them easier to process [52]. Because of these properties, thermotropic polymers are used for the

production of composites due to their ability to enhance structural and non-structural functions such as strength and thermal stability [48, 53]. Also their tendency to orient makes them ideal for a variety of processing techniques such as extrusion or injection molding [50, 54].

2.3 Polymer processing

2.3.1 General techniques

The processing of polymers and composites has been characterized by a wide diversity of methods and techniques, where the most common are: post die processing, forming, injection molding and extrusion [55]. From these, extrusion is the most used technique for polymer processing in industry and for research purposes in academy [56-58]. The selection of a specific technique depends on the type of material that is going to be processed, its complexity, and the required properties of the product as well as the processing costs.

Post die processing can be divided in fiber spinning, film blowing and sheet forming [59]. These processes are characterized for being free-surface where shape and thickness of extrudate is strictly determined by the rheological properties of the

melt. These techniques, especially film blowing shown in Figure 4a, are amongst the most important in the polymer processing industry [60]. The forming process is composed of three techniques: blow molding, thermoforming and compression molding. Blow molding is typically used for the production of hollow objects, such as containers, automobile bumpers and duct work [61]. It consists in inflating a piece of polymer by an open ending, generally after an extrusion, with compressed air until it fills a mold cavity.

Thermoforming consists in heating a polymer sheet and pressing it into the bottom of a mold by means of mechanical force, pressure or vacuum [62], as shown in Figure 4b. In the case of injection molding it consists on feeding a material into a heated barrel and forced into a mold cavity by a hydraulic system where it cools and takes the mold shape.

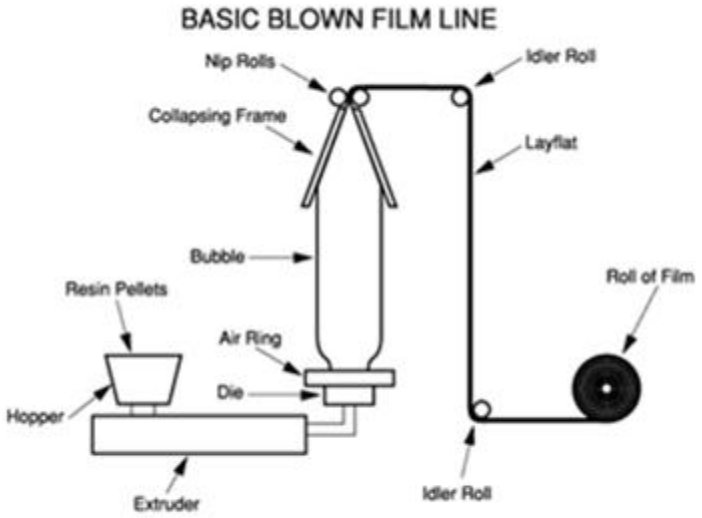

(a)

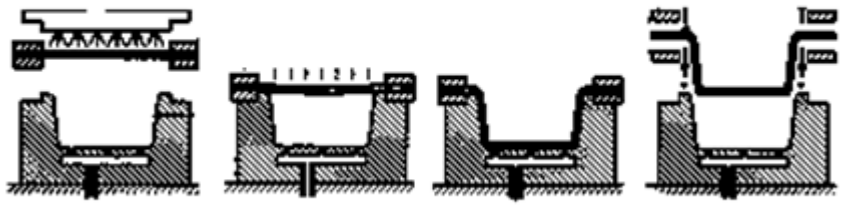

(b)

Figure 2.4 Schematic diagram of (a) film blowing and (b) thermoforming.
Reproduced from reference [63].

2.3.2 Extrusion

As mentioned before, the extruder is the device most commonly used for polymer processing. The extrusion technique consists on pushing a material through an opening, called die, of predetermined cross-sectional area. The geometry of the die, as well as the material flow properties and the flow rate, determines the pressure needed to perform the extrusion. In the case of thermoplastics, when a screw extruder is used, the feed polymer is heated until it melts in order to reach a fluid state and make the pumping through the die easier. Then the product (i.e. polymer, composite) is solidified by cooling after it exits the die. To operate an extruder, melt pressure, screw speed and temperature have to be monitored. This technique is commonly used for fluids ranging from medium to high viscosity, such as oils, food stuff, and polymer melts. Some examples are those studied by Kartika [57] and coworkers for the extraction and processing of sunflower seed oil. While Liang also studied the viscosity of polymers during extrusion [64]. Extrusion is also regularly used for research purposes, such as in the case of Xifeng Xu and colleagues on their study of poly(ethylene terephthalate)/clay nanocomposites [65]. In this studies they stated that the extrusion method played an important role due to its simple and versatile processing way. Also, Campell and McNally preferred the extrusion technique for the

production of poly(ethylene glycol) nanocomposites for drug release because this technique can be easily transfered from batch processing to a continuous process [66].

The most common extruders used are single and twin screw extruders. Examples of single and twin screw extruders are shown in Figure 5a and 5b respectively.

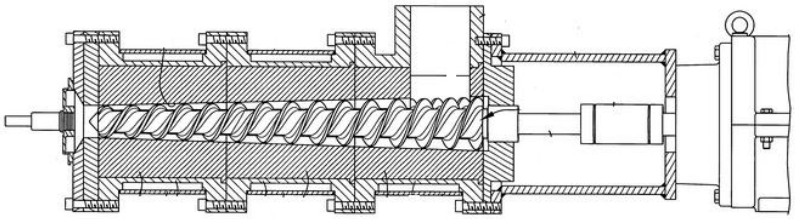

(a)

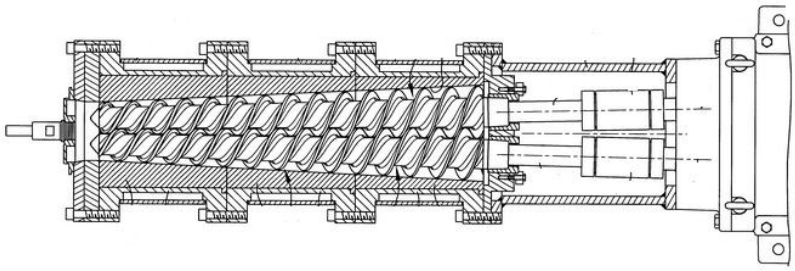

(b)

Figure 2.5 Schematic diagram of (a) single screw extruder and (b) twin screw extruder.
Reproduced from reference [38].

Single screw extruders, as the name implies, consists of one rotating screw, which its main function is to melt and pump the material. Single screw extruders also find applications in the food industry as mixers and moisture or volatile components remover [67, 68]. Material transport in this type of extruders is drag-induced and flow is determined by frictional properties of the solid and melted phase.

In the case of twin screw extruders its classification depends on the degree of screw intermeshing and the direction of screw rotation. These classifications are as follows: co-rotating or counter-rotating by screw rotational direction, and intermeshing, non-intermeshing and self-wiping by screw arrangement and vicinity.

This type of extruders are greatly used in academy and industry since they are capable of processing materials with high viscosities or materials that cannot be easily processed in single screw extruders due to the limitations in the development of shearing forces. Kuiper and coworkers made a critical study comparing single and twin screw extruders for different food applications where they determined that for highly viscous food materials a better mixing was obtained in a twin screw extruder [58]. Russo and coworkers [69] used single and twin screw extruders to measure the rheological and mechanical properties of nylon 6 nanocomposites and reported that structural and performance modifications were highly dependent on matrix degradation and filler amount. In addition to thermal degradation, another disadvantage that may

be present in extrusion are the detrimental effects due to the high shear forces that take place, such as sharkskin or surface mattness and melt fracture.

To describe the shear rate in a screw channel it is assumed that the geometries are the same as in a coaxial cylinder set-up and the surfaces (screw and barrel) are flat plates (same as for a Couette geometry). Also it is assumed that the barrel rotates relative to the screw as this gives better results, described by Equation 2 where D is the outside diameter of the screw, N is the rotational speed of screw and H is the channel depth. The shear rate of the polymer melt between the screw flight and the barrel is described by Equation 3, where δ is the flight clearance. After these assumptions the shear rate as stated by Rauwendaal is [70]:

$$\dot{\gamma}_{ch} \cong \frac{\pi DN}{H} \qquad \text{Equation 2}$$

and

$$\dot{\gamma}_{cl} = \frac{\pi DN}{\delta} \qquad \text{Equation 3}$$

A schematic of a screw in a channel is shown in Figure 6.

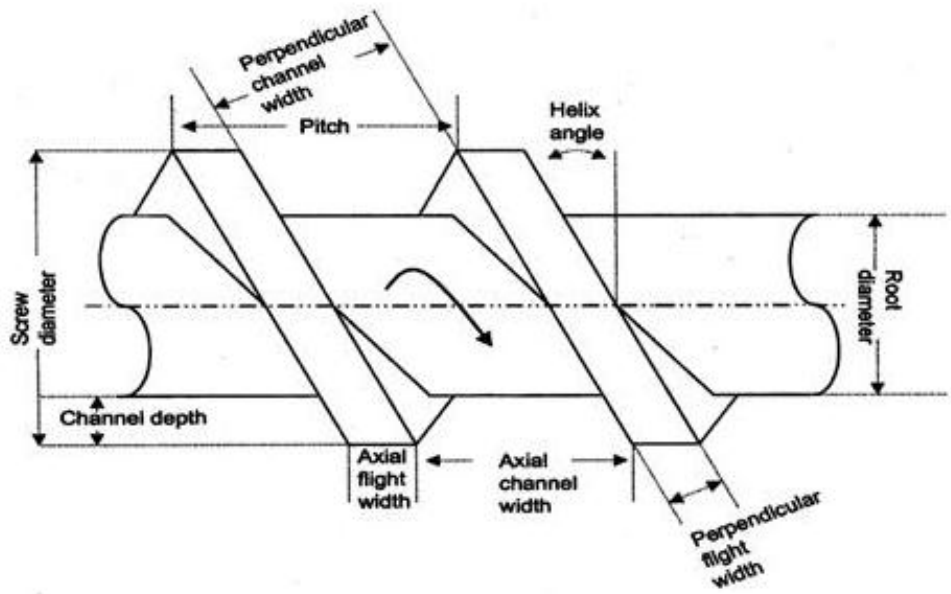

Figure 2.6 Schematic diagram of an extrusion geometry.
Reproduced from reference [71].

Another important part of the extrusion process is the flow behavior within or through the slit die, which is represented in Figure 7, where the direction of mass flow is on x direction.

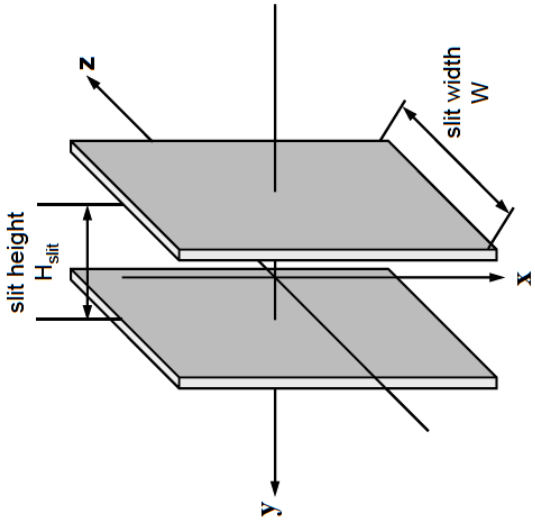

Figure 2.7 Schematic of slit die.
Repreduced from reference [72].

In the case of polymer melts the velocity profiles are not parabolic, but they do follow the velocity distribution of Ostwald – de Waele, Equation 4, which describes a power law fluid. Where v_0 is the maximum velocity (v_{max}) at y = 0 (center line) while H_{slit} is the channel height, n is the flow exponent defined as k + 1. Here k is the slope of the shear viscosity function. Finally, v_{slip} is the slip velocity at the wall.

$$v_x(y) = v_{slip} + \left(v_0 - v_{slip}\right)\left[1 - \left|\frac{2y}{H_{slit}}\right|^{\frac{n+1}{n}}\right] \qquad \text{Equation 4}$$

For Newtonian fluids the flow exponent (n) is equal to 1, while for shear thinning fluids n is always smaller than 1.

Figure 8 shows a flat shaped region is at the middle of the channel, which is typical of polymer melts.

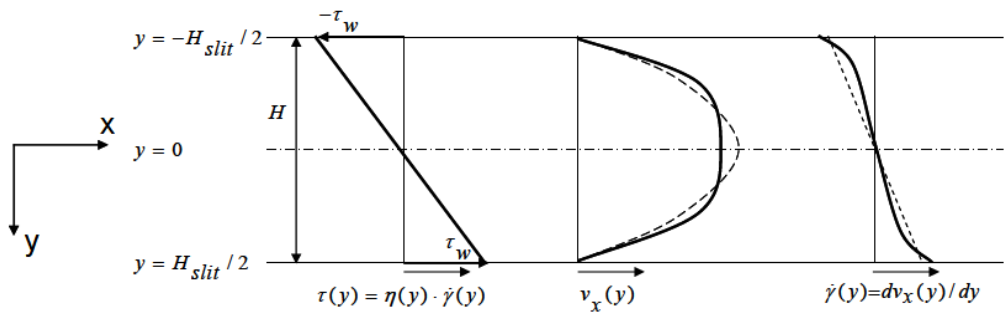

Figure 2.8 Shear stress, velocity and shear rate distribution of a Newtonian (dashed line) and shear thinning (solid line) material in a slit die.
Reproduced from reference [72].

For shear thinning fluids, the true stress can be calculated using the Weissenberg and Rabinowitsch equation, Equation 5, where D_w is the apparent shear rate at the wall for Newtonian fluids.

$$\gamma_w = D_w\left(\frac{2}{3} + \frac{1}{3} \bullet \frac{d \log D_w}{d \log \tau_w}\right), \; D_w = \frac{6m}{\rho H_{slit} W} \qquad \text{Equation 5}$$

Where m is the mass flow, ρ is the density of the fluid, W is the slit width and τ_w shear stress at the wall.

2.3.3 Melt rheology

Rheology is concerned with the deformation of materials under the influence of stresses. Deformation and flow are present when polymers are softened or melted and then reformed into solid products of different shapes. In the case of polymer melts or viscoelastic materials, when subjected to an external deformation, the natural response is to remain between a viscous liquid and an elastic solid. The viscoelastic properties are dependent on many variables, including temperature, pressure and time, among others.

The rheological behavior of polymer melts is strictly influenced by the entanglements (i.e. molecular crossovers) in its chains since they provide resistance to deformation. Even small differences in chain entanglements represent large differences in the flow behavior and these differences can be measured by rheological tests due to its sensitivity. Rheological measurements are used as an effective tool for: quality control of raw materials, predicting material performance, and manufacturing processes [73]. Polymer melts show a shear thinning behavior, which is due to the alignment and disentanglements of the polymer chains. In the case of TLCP's the behavior is even

more complicated than for flexible polymers due to the existence of polydomain structures. Some studies performed by Kim and colleagues showed that the complex viscosity $|\eta^*|$ decreased as a function of frequency in TLCP's nanocomposites [74]. In the case of filled polymers, the presence of particles affects the rheological characteristics of the polymer system due to the size, shape and concentration. There are a numerous of articles that study the rheology of filled polymers [75-78].

An important viscoelastic response in polymers is the normal stress, which is related to extrudate swell. As the name states, normal stress is a force perpendicular to a surface. In extrusion, a fluid is forced to flow through a conduit where it exerts both, normal and shear stresses. But once the material exits the die the normal stresses are released which translates in swelling. This behavior may represent some problems for the product manufacture and can be eliminated by studying the rheological behavior of such materials.

2.4 Particle Dispersion

Dispersion in nanocomposites is always a matter of concern because it is the most important requirement for achieving the so-called enhancement of the properties. But it is important to point out that a good dispersion means that the physical, thermal and/or mechanical properties do not vary spatially at the macroscopic level, which

suggests that the nanoparticles are either randomly or uniformly distributed. Uniform dispersion of the nanoparticles produces a large interfacial area per unit volume between the nanoparticles and the host polymer. A large amount of articles deal with the fact of dispersion in nanocomposites and agree that there has to be an attractive interaction between the nanoparticles and the matrix to avoid agglomeration [79-81]. Thus, nanoparticles may be surface treated to provide hydrophobic characteristics and enhance inclusion into a hydrophobic polymer matrix [25]. This suggests a cautious study of polymer crystallinity and chemistry, molecular weight, and synthesis methods. Such is the case when the nanoparticles used are carbon nanotubes (CNT's), where the functionalization will be an effective method to achieve a uniform dispersion due to interfacial adhesion improvement between matrix and particle.

In the case of clay nanoparticles they are generally functionalized or modified by ion exchange reactions of organophilic cations in order to obtain a good dispersion ranging from intercalated to exfoliated [82]. That is the case of Huang and Han who suggested that organoclay nanocomposites present some problems of dispersion due to the lack of compatibility between the polymer matrix and the organoclay [83].

In the case of melt mixing for polymer nanocomposites particle agglomerates undergo dispersion by two mechanisms: rupture and erosion. A study performed by Kasaliwal and colleagues [79]. found that at low mixing speeds the dispersion was

dominated by both mechanisms, while rupture mechanism governed at higher mixing speeds. Rupture is considered a bulk phenomenon and erosion is considered a surface phenomenon. In the first one (rupture) large agglomerates are broken in short times and in the case of erosion small components from the surface agglomerate are slowly eroded. The later requires longer times to achieve a good dispersion, yet it will cause less damage to the nanoparticles. Rupture mechanism can cause defects on the surface of the nanoparticles due to the high intensities of the shear forces. That is why different tests or processing parameters have to be performed in order to have a balance between particle dispersion without causing particle or surface damage.

3. MATERIALS AND METHODS

3.1 Polymer matrix

The polymer matrix used in this study was poly (4-hydroxy benzoic acid-co-ethylene terephthalate) (PHBA/PET). It was purchased from Sigma Aldrich (Batch # 02203MO, Cat. # 531235-100G) and the structure of the copolymer is shown in Figure 9, where m and n are 60 and 40 respectively. The advantages that encouraged the selection of this polymer are its relatively low cost and availability, but most important because it is a copolymer with rigid segments that shows a nematic phase which have shown to have no significant die swelling [84, 85]. The procesability of liquid crystalline polymers (LCP's) is enhanced by the low viscosity in the nematic melt phase, which in PHBA/PET is markedly present around the range of 250 – 300 °C. Also, the nature of this polymer makes it more stable at elevated temperatures and have better mechanical properties when compared to flexible polymers [86, 87].

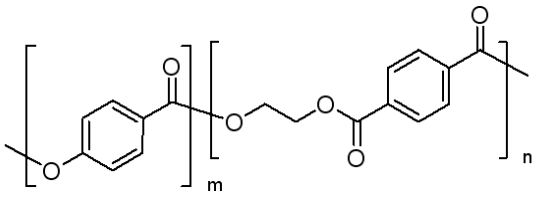

Figure 3.1 Chemical structure of the PHBA/PET molecule.

This is the same aromatic polyester as developed by Jackson and Kuhfuss and investigated by many other researchers, it is also important to mention that it is a thermotropic [36]. The liquid crystalline behavior is present due to the HBA segments, which are the rigid part of the copolymer. ET segments are the flexible segments in the copolymer, which are added to the HBA in order to lower its melting point since it is virtually impossible to process the PHBA unit alone by conventional methods [87]. Different ratios of this copolymer were synthesized and studied in order to find the correct balance of enhanced properties. The 60:40 molar ratio proved to have better mechanical properties and processing characteristics than the other ratios [87]. Liquid crystalline polymers are stronger than flexible polymers due to the orientation of the molecules, which promotes the formation of fiber-like structures. This behavior also makes them more stable at higher temperature and provides better chemical stability among.

3.2 Nanoparticles

Different shapes of nanoparticles were evaluated in order to determine the effect of particle shape and concentration on the polymer matrix.

Multiwalled carbon nanotubes:

Carbon nanotubes (CNT's) are known for having excellent mechanical, electrical and magnetic properties. Due to its high aspect ratio they are also used as reinforcing agents to produce high strength polymer composites. The cylindrical morphology of the CNT's promotes the formation of networks, which also helps in the strengthening of the matrix.

Some researchers have demonstrated that despite a poor dispersion, small filler loadings improve substantially the mechanical, thermal and electrical properties. CNT's promote the formation of a percolated network that helps either in the mechanical, electric and/or heat conduction, thus enhancing the electrical or thermal properties. Because of the cylindrical geometry, MWCNT have the tendency to increase the strength compared to the neat matrix due to the formation of fiber-like structures at the break surface. The formation of this network helps to prevent crack propagation in the matrix due to the constant change in direction of the stress or deflection of the evolving crack.

The multiwalled carbon nanotubes (MWCNT's) used in the studies presented herein were carboxylated to enhance particle affinity with the matrix and were purchased from CheapTubes [88], having an outside diameter of 8 nm and a length of approximately 10-30 μm.

Clays (Halloysite and Montmorillonite):

Clays are naturally occurring materials composed of phyllo silicate minerals and are known as good fire and heat retardants. Their crystal structure consists of aluminum or magnesium hydroxide octahedral sheets sandwiched between two silicon oxide tetrahedral sheets. They are used as fillers for the production of polymer composites where different applications and enhancements have been found. A typical example is the use of clays for barrier layer applications (i.e. bottles) due to their efficiency on slowing down the path of gases and liquids. The reason for this is that clay nanoparticles increase the tortuous path through the polymer matrix due to the galleries in its structure and the morphologies adopted when dispersed in a polymer matrix. The morphologies adopted may be, aggregated, intercalated, flocculated or exfoliated. The halloysite nanoclays (HNC's) used had a diameter of approximately >100 nm and lengths of 500-1.2 μm and were purchased from Sigma Aldrich (Batch #09514DJ, Cat. #685445-500G). In the case of montmorillonite nanoclays, which are

plate-shaped, the dimensions are L ~ 1 μm and thickness of about 1-3 nm. They were also were purchased from Sigma Aldrich (Batch # 03717JH, Cat. #682632-500G).

Silica:

Silica nanoparticles have a spherical geometry with the chemical formula of SiO_2, as shown in Figure 10. These kinds of nanoparticles can be obtained as monodisperse, which has been reported to be an advantage for the enhancement of mechanical properties in composites[11]. It is also the most abundant mineral in soil and this makes it very accessible. The motivation for using silica as a matrix filler is due to its spherical shape which will give us the opportunity to compare the impact of spherical shapes with the other geometries used. Silica can be also easily synthesized or economical, if purchased. In this case, silica nanoparticles were purchased from Sigma Aldrich (Batch # 05812MD, Cat. # 637238-50G) and have a D ~15 nm and a purity of 99.5 %. They are porous and amorphous.

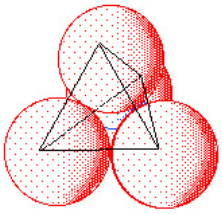

Figure 3.2 Schematic of SiO_2 molecular structure.

3.3 Nanocomposite preparation

Nanocomposite films where produced by direct melt blending in a co-rotating intermeshing twin screw extruder (Haake MiniLab II) with a 5/14 mm conical screw and a length of 109.5 mm, shown on Figure 11.

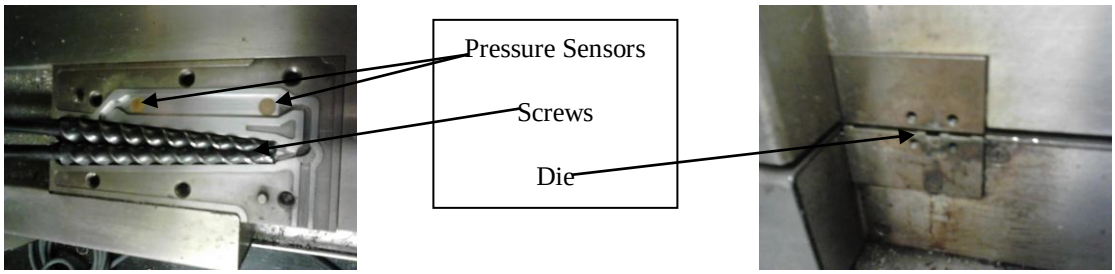

Figure 3.3 Schematic of twin screw extruder and die exit.

Polymer pellets and fillers are slowly fed to the extruder for approximately ten minutes at 290 °C while screws were set at 10 rpm in order to perform a pre-mixing and most important, to avoid material accumulation at the hooper. The melt was processed at 40 rpm and 300 °C and extruded at 190 °C and 10 rpm. Extrusion was carried out through a rectangular die of 4.0 mm by 1.0 mm (W x H). It is important to mention that the product is naturally quenched when exposed to ambient temperature immediately after extrusion. The extrudate is collected over a D22 transport conveyor belt (0 – 50 mm/s) which is manually manipulated in order to match the exiting flow rate to obtain uniform samples.

3.4 Characterization

Digital scanning calorimetry (DSC):

One of the thechniques for thermal characterization is DSC, which is used as a complementary tool to optical microscopy. The DSC reveals the presence of mesophases and liquid crystal phases by detecting the enthalpy change associated with a phase transition. Although the calorimetry cannot identify the type of phase, some useful information about the degree of molecular ordering within a mesophase can be derived on the basis of the level of enthalpy change.

The analyses performed on the composites consisted in weighing samples of approximately 10 to 15 mg which were deposited in a T_{zero} aluminum pan and sealed with a T_{zero} hermetic lid. Care was taken in order to ensure that the sample to be analyzed touched all or most of the pan's bottom, for better or most reliable data acquisition. The instrument used was a Q-2000 differential scanning calorimeter from TA Instrumens and the parameters for sample testing where set using a ramp in standard mode from 20 to 420 °C at a heating rate of 5 °C/min in a dry air atmosphere and with a nitrogen flow of 50 mL/min to cool the system.

Thermogravimetric analysis (TGA):

TGA consists in the determination of sample weight loss with temperature changes. It is commonly used in the characterization of polymers to determine degradation temperatures, absorbed moisture, and level of inorganic and organic components in sample. With this characterization technique the determination of composite decomposition displacement as function of particle loading and/or morphology is more accurate [45].

Non-isothermal analyses were carried out using a TA Instruments Q-2950 thermo gravimetric analyzer. Samples ranging from 20 to 30 mg were loaded on an aluminum pan and heated at a rate of 5 °C/min from 20 °C to 600 °C. Air flows of 60 mL/min and 40 mL/min were used for the sample and reference chambers respectively.

TGA data was analyzed using the TA Universal Analysis 2000 software in order to determine the maximum degradation temperature and rate of degradation.

Small angle x-ray scattering (SAXS):

SAXS is used to obtain information from unidirectional samples about the orientation of the molecules and nanoparticles in order to identify liquid crystalline structures (for our purpose). Typical angles studied range between 0.1 and 5 degrees were the smallest accessible angle gives the largest resolution feature size. This technique is applicable to crystalline and amorphous materials and sample preparation is relatively easy.

Small angle x-ray scattering patterns were recorded using an attachment for SAXS in a Rigaku Ultima III θ-θ goniometer unit with a CuK_{α} target (λ= 1.5418 Å). The anode was operated at 40 kV and 44 mA. Also a div. slit and high limiting (H.L.) slit of 1.0 mm and 10.0 mm, respectively, were used along with a sample holder attachment for transmission method. A scanning speed of 0.05 °/min at steps of 0.05° was used to obtain patterns for each sample from 0.6 to 1.5° (2θ).

Polarized Optical microscopy (POM):

The use of microscopy is the most direct technique for obtaining structured information. This technique uses visible light and lenses to magnify images of small size. It can be used to analyze samples and probe length scales down to around 0.5 μm and even smaller if light is collected in the near field, where textures and macro structures can be observed.

This technique was implemented in order to identify the nematic phase range. To analyze the samples a thermal hot stage was set at 300 °C. The nematic phase of the sample was reached and a water bath was used to eventually chill the system. Lens having a magnification of 10X was used to take the photos along with a Cannon professional camera. Samples were cut using a surgical blade from surface to inner sections in order to have a representative behavior of the whole composite.

Scanning electron microscopy (SEM):

This technique consists in scanning the sample surface with a high energy beam of electrons which can reach scale lengths of approximately 15 Å. The interaction of the electrons with the sample may provide information of surface topography and composition.

Scanning electron micrographs were obtained using a JEOL-JSM-6930LV scanning electron microscope and employing an accelerating voltage of 5 and 10 kV.

Composite samples were randomly broken in order to obtain surface cracking and then were coated with gold in a spun coater for approximately 2 minutes as stated for low conductive samples. Sample pieces were placed over a carbon glue grids and aluminum pan holders to study its cross sectional fracture plane.

4. EFFECT OF ROD-LIKE PARTICLE ON THE STRUCTURE AND THERMAL PROPERTIES OF THERMOTROPIC LIQUID CRYSTALLINE POLYMER NANOCOMPOSITES

4.1 Introduction

Liquid crystalline polymers (LCP's) have been studied in the last decades for different engineering applications as potential matrices for the production of lightweight composites [89, 90]. Among this kind of polymers, thermotropic LCPs are considered as one of the high-performance engineering thermoplastics, especially for those that present the nematic structure at the melt state [91]. Nematic polymers have excellent mechanical properties and high-temperature stability [80]. These properties are related to the rigidity that the aromatic rings gives to its structure along with the ester linkages. The combination of these characteristics promotes a low melt viscosity behavior at the melt state, which also makes them relatively easy to process.

Nano and micron size particles are added in order to enhance the matrix, but this may also affect the anisotropic properties of the LCPs. The fillers used in this section had a rod-like morphology in order to study the effect of these particles on the structure and thermal properties of extruded 60:40 mol % poly(4-benzoic acid-co-ethylene terephthalate) composite strips with varying filler concentration. It is our

belief that rod-like reinforcements will tend to orient more easily in the nematic phase and this could be related to a possible improvement in mechanical properties, as well as electrical and heat conduction along the flow direction, which will be the matrix/filler preferential direction. These kinds of systems show a fibrillar behavior at the fracture surface when observed by the SEM technique; which is related to mechanical property enhancement as there is a resistance to crack propagation. In addition, liquid crystalline structure was studied by the use of polarized optical microscopy (POM) in the nematic range and by small angle X-ray scattering (SAXS) to determine if there was any effect in the crystalline arrangement or lattice ordering which could be evidenced by differences in peak position or curve intensities.

Liquid crystalline transition range showed to be reduced as isotropic-to-nematic characteristic temperature diminished while melting point remained almost constant for HNC and with a slight increment for MWCNT. While temperature resistance or composite decomposition was mostly favored by HNC since decomposition temperatures for MWCNT composites remained almost unchanged.

4.2 Thermal characterization – TGA

Since PHBA/PET is a copolymer it has two weight loss stages during degradation, where the first major degradation occurs in the range from 300 to 350 °C and the second one appears around 450 °C. The first stage of degradation is mainly due to the decomposition of the PET units while the second stage is attributed to the decomposition of the PHBA blocks. During the first degradation it has been identified that CO, CO_2, phenol and ethylene, among other aliphatic compounds, were evaporated. At higher temperatures, near 600 °C, great intensities of CO_2, phenol and other minor components of HBA, such as benzoic acid have been reported [45].

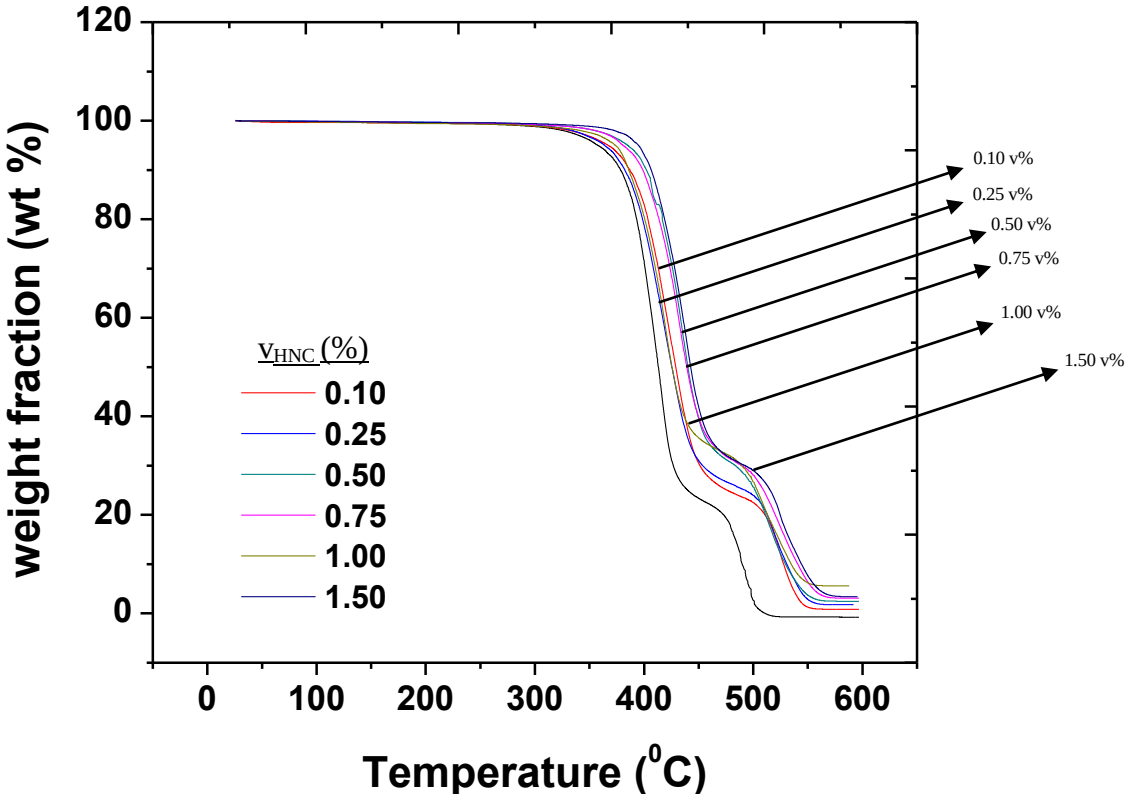

Figure 4.1. Thermogravimetric characterization of PHBA/PET and HNC nanocomposites.

From 20 ºC to 600 ºC at a rate of 5 ºC/min under air atmosphere.

Our results show that the incorporation of HNC improves composite thermal stability as an evident displacement of the degradation stages is observed in Figure 4.1. Clays are known for being good heat retardants having a thermal conductivity constant of 0.25 W/mK without moisture [92, 93]. Also these hollow-like clays act as good heat delayers and as physical barriers for decomposition products which try to escape when volatilized. This behavior also suggests a good interfacial adhesion between filler and matrix since the thermal motion of the polymer molecules is evidently restricted; limiting polymer relaxation as temperature is increased; which translates as improved thermal properties.

TGA analysis show that degradation temperatures, reported at 5 wt% (T_5) and 10 wt% (T_{10}) of loss, as well as the temperature of maximum rate of weight loss (T_{md}), are increased and for some cases (< 0.25 v%) by an approximated Δ of 10 °C or more. A summary of results is shown in Table 4.1.

Table 4.1. Effect of HNC fillers on the thermal stability of the PHBA/PET nanocomposite

HNC (v %)	T_5 [a] (°C)	T_{10} [b] (°C)	$T_{md\,1}$ [c] (°C)	$T_{md\,2}$ [d] (°C)
Neat	357.6	378.2	412.2	490.5
0.10	367.1	386.9	421.2	521.2
0.25	363.8	382.1	421.7	524.8
0.50	385.2	402.2	433.4	513.8
0.75	380.7	398.9	431.3	522.5
1.00	373.8	385.9	428.8	518.7
1.50	394.9	406.5	439.4	526.1

a - Temperature at a weight loss of 5 % b - Temperature at a weight loss of 10 %
c - Temperature at 1st maximum of 1st derivative d - Temperature at 2nd maximum of 1st derivative

As evidenced, there is a thermal enhancement with addition of HNC since degradation temperatures are displaced to relatively higher values when compared with the neat matrix. Degradation temperatures were displaced between 6 and 37 ºC and between 4 and 28 ºC for 5 & 10 % of weight loss respectively. While the temperatures at the maximum degradation rate for the first and second stage were displaced between 9 and 27 ºC and between 26 and 36 ºC, respectively.

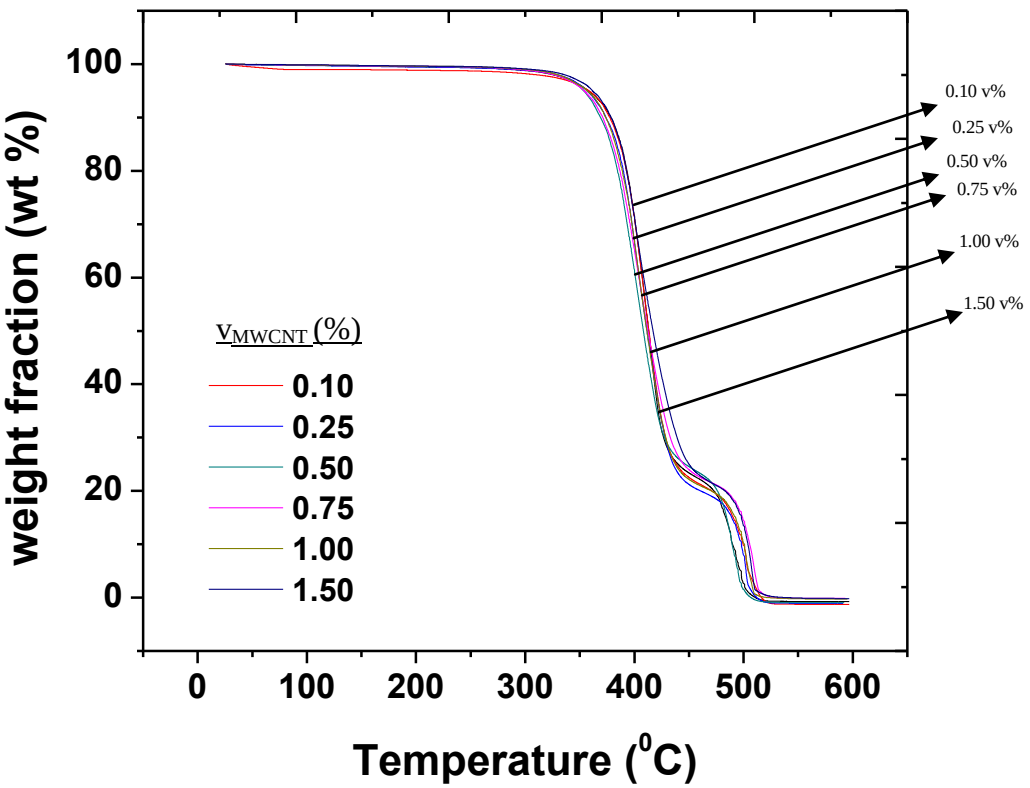

Figure 4.2. Thermogravimetric characterization of PHBA/PET and MWCNT nanocomposites.

In the case of MWCNT fillers, whose thermal conductivity constant is approximately 15 W/mK, the effect is slightly differen. No clear tendency is seen in order to differentiate the neat matrix from the composites in the TGA curves as observed in Figure 4.2.

Addition of MWCNT does not seem to have any effect on T_5 and T_{10} since they remain almost constant no matter what the filler concentration. While T_{md1} decreases systematically as filler concentration increases, the maximum change in temperature is approximately 27 °C (i.e. 1.5 v% vs neat). In the case of T_{md2}, there is also an increment in temperature as MWCNT are added but it is not systematic. As shown in Table 4.2, T_{md2} reaches a peak at a concentration of 0.75 v% and then drops to a constant value of 505 °C. This behavior may suggest that MWCNT are not well dispersed at these higher concentrations or at least they are not as dispersed as in the lower concentrations since a systematical increase should be expected. Also, these results (specifically T_{md}'s) show that there is a tendency of promoting the first stage degradation (i.e.PET rich phase), while the second stage still has an increasing trend. While a slightly different effect is observed for the MWCNT, when compared to the HNC, since no clear tendency is seen in order to differentiate the neat matrix from the

composites in the TGA curves. Some researchers have reported that the decomposition of PET units occurs due to the rupture of ester linkages followed by the transformation of the carboxylic groups to olefinic ends by the transfer of H [84]. HBA has a slightly acid environment which may be attractive for the MWCNT to link, this suggest an improvement of PHBA-rich phase while negatively affecting PET-rich phase. On the other hand, it seems that the PET blocks are more likely to attract MWCNT since the carboxyl groups will easily interact with the polarized oxygens. This interaction may happen at the flexible side of the PET chain which may limit the molecule or bond flexibility, promoting rigidity which in fact will result in the "scission" or bond rupture of this link.

Table 4.2. Effect of MWCNT fillers on the thermal stability of the PHBA/PET nanocomposite.

MWCNT (v%)	T_5[a] (°C)	T_{10}[b] (°C)	$T_{md\ 1}$[c] (°C)	$T_{md\ 2}$[d] (°C)
Neat	357.6	378.2	412.2	490.5
0.10	356.7	375.8	410.7	500
0.25	356.6	373.8	407.8	506.4
0.50	356.8	368.8	407.3	496.1
0.75	353.9	371.0	406.4	512.7
1.00	353.8	373.7	405.0	505.2
1.50	353.8	376.8	401.3	505.0

a - Temperature at a weight loss of 5 % b - Temperature at a weight loss of 10 %
c - Temperature at 1st maximum of 1st derivative d - Temperature at 2nd maximum of 1st derivative

4.3 Thermal characterization – DSC

DSC experiments show that the PHBA/PET copolymer has three thermal transitions before degradation; these are at approximately 52 °C (endothermic), 175 °C (endothermic), and 300 °C (exothermic) as shown in the DSC curves in Figure 4.3 and 4.4 for MWCNT and HNC, respectively. Other researchers [94, 95] report that temperatures around 50 to 70 °C are attributed to a glass transition, while the one from

170 to 185 °C are due to melting of crystallites, and the one in the range from 300 to 360 °C corresponds to the formation of a nematic phase [35, 85].

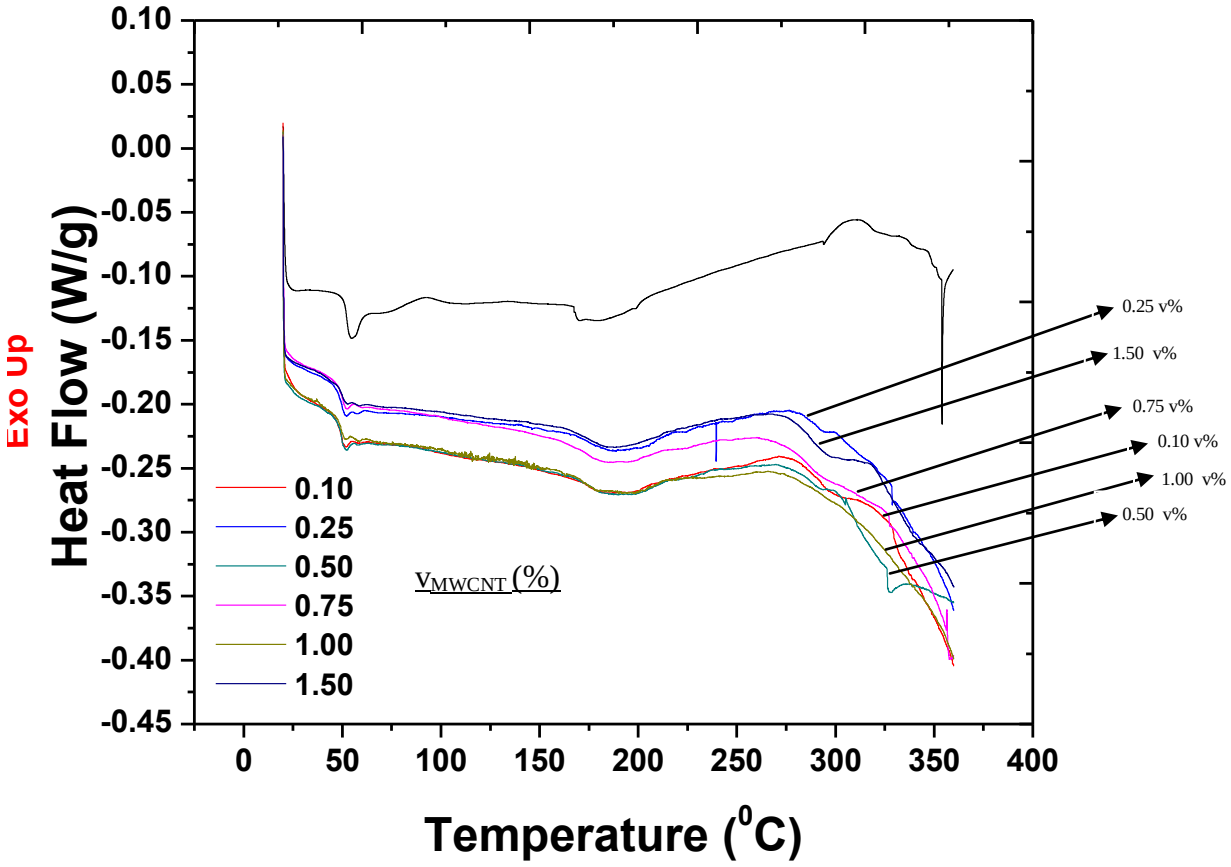

Figure 4.3. DSC thermograms of PHBA/PET and MWCNT nanocomposites.
From 20 ºC to 360 ºC at 5 ºC/min.

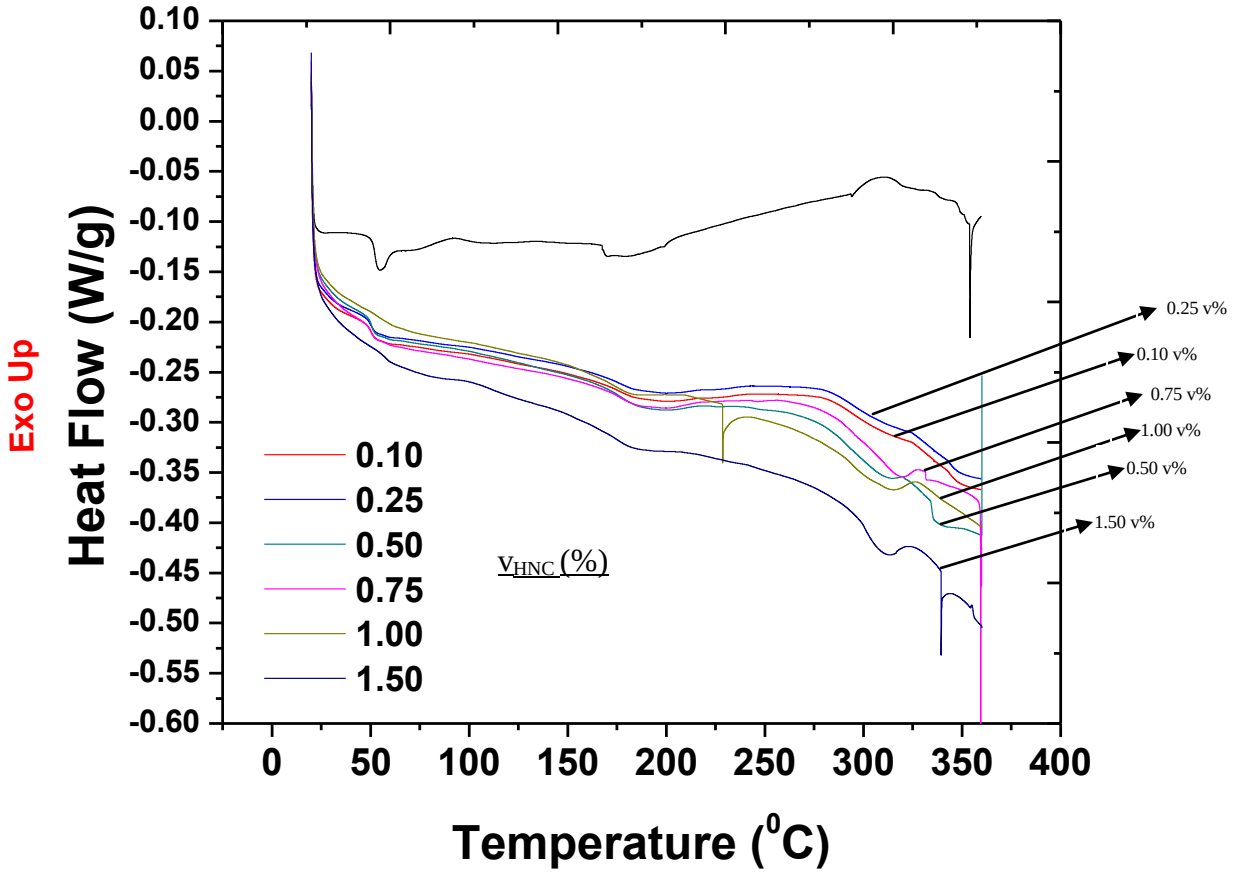

Figure 4.4. DSC thermograms of PHBA/PET and HNC nanocomposites.

.

Addition of MWCNT slightly broadens the polymer transitions, but softens the DSC curves at transitions. Which means that the abrupt changes are kind of masked when compared to the neat matrix. In the case of HNC it is clearly seen that addition of these particles broadens and also softens the curves at the thermal transitions. But most relevant, composite heat absorption is enhanced when compared to the neat matrix for both kinds of rod-like nanoparticles. In order to quantify and have a better explanation of this behavior the thermal transitions of the DSC curves were studied to see how the enthalpies of every transition where changing and why this broad/softening behavior was taking place. Tables 4.3 and 4.4 show how the enthalpy of transitions changed as a function of temperature and concentration for the MWCNT and HNC fillers, respectively.

Table 4.3. Transition enthalipies for PHBA/PET MWCNT composites.

MWCNT (v %)	ΔH_g * (J/g)	ΔH_m * (J/g)	ΔH_{IN} * (J/g)
Neat	1.01	3.54	1.25
0.1	0.607	3.69	1.20
0.25	0.515	4.13	0.896
0.5	0.589	4.66	2.06
0.75	0.564	4.47	1.00
1.0	0.307	4.55	0.926
1.5	0.203	5.53	0.714

ΔH_g – glass transition ΔH_m – melting point ΔH_{IN} – isotropic to nematic phase

*Average values taken from a total of n=3 measurements.

The energy requirement for the glass transition of MWCNT composite is reduced, by an amount of 0.807 J/g, comparing the 1.5 v% vs neat, which could be attributed to a better dispersion when compared with HNC. The energy at the melting point is almost systematically increased as the MWCNT concentration increases. At this stage of high molecular deformation, energy is absorbed by the polymer molecules as well as by the fillers. For the glass temperature is different, since at this stage the change in volume as temperature changes is vigorous.

Table 4.4. Transition enthalipies for PHBA/PET HNC composites.

HNC (v %)	ΔH_g * (J/g)	ΔH_m * (J/g)	ΔH_{IN} * (J/g)
Neat	1.01	3.54	1.25
0.1	0.767	2.39	1.18
0.25	0.978	3.21	1.08
0.5	0.866	4.66	1.05
0.75	0.723	4.85	0.883
1.0	0.945	5.99	0.971
1.5	0.800	6.42	0.961

ΔH_g – glass transition ΔH_m – melting point ΔH_{IN} – isotropic to nematic phase

*Average values taken from a total of n=3 measurements.

The energy requirement to promote molecular relaxation at the glass transition only shows a slight decrease can be observed. This decrease may be attributed, at these relatively low temperatures, to the presence of dispersed fillers which will contribute to the increment in molecular volume which also increases molecular deformation. Glass temperature is when polymer molecules are undergoing some relaxation by changing its molar volume with a change in temperature. A similar behavior is observed for the isotropic to nematic transition, but this transition is exothermic which means less energy is released as particle concentration increases. This may be an indication of nematic phase promotion as rod-like fillers are added.

The temperatures reported in Tables 4.5 and 4.6 are the temperatures at the minimum of the peak in the DSC curve for the first and second transitions (i.e. glass temperature and melting point, respectively). These transitions need more energy absorption in order to promote some molecular re-ordering and crystal flow. While the temperature of the third transition (nematic phase) is the maximum of the peak in the DSC curve, it is the maximum since this kind of transitions where some order or liquid crystallinity is promoted are characterized for being exothermic.

Table 4.5. Effect of MWCNT fillers on the glass, melting and I-N transition temperatures of the PHBA/PET nanocomposite.

MWCNT (v%)	T_g * (°C)	T_m * (°C)	T_{IN} * (°C)
Neat	52.5	184.2	330
0.10	53.0	185.3	318.7
0.25	53.0	192.4	301.0
0.50	52.8	194.9	296.9
0.75	53.2	186.2	293.1
1.00	52.2	186.9	304.7
1.50	53.5	191.0	306.7

T_g – glass transition T_m – melting point T_{IN} – isotropic to nematic phase

*Average values taken from a total of n=3 measurements.

For MWCNT, the glass transition remains almost constant with a variation of approximately ± 2 ºC as shown in Figure 7.1, while the melting point seems to increase as a function of particle concentration but the temperature values remain inside the error range as shown in the same figure. The isotropic to nematic transition is significantly reduced by approximately 23.3 ºC, but the values remain also inside the error range which could represent that there are no significant changes. The range from glass transition to melting point tends to increase with the addition of MWCNT; increasing by 6 to 8 ºC which is not very attractive from a material processing point of view due to the energy consumption. In the case of the isotropic to nematic transition range the temperature gap is reduced almost systematically as MWCNT concentration increases.

Table 4.6. Effect of HNC fillers on the transition temperatures of the PHBA/PET nanocomposite.

HNC (v%)	T_g * (°C)	T_m * (°C)	T_{IN} * (°C)
Neat	52.5	184.2	330
0.10	52.4	184.2	322.0
0.25	53.8	188.06	314.8
0.50	53.2	185.5	314.1
0.75	55.0	184.0	314.7
1.00	54.5	178.9	311.5
1.50	59.8	182.7	312.3

T_g – glass transition T_m – melting point T_{IN} – isotropic to nematic phase

*Average values taken from a total of n=3 measurements.

Thermal transitions for HNC show an increment of approximately 7 ºC while the melting point tends to stay almost constant. This is an indication of HNC adding or helping in the polymer chain relaxation at the early stages of heating. This is a good signal for material processing since it translates into less energy requirement for composite production. In the case of isotropic to nematic transition, the characteristic temperature is greatly reduced by approximately 18 ºC. This is the same as saying that the isotropic to nematic range decreases as HNC concentration increases. HNC particles help in promoting composite orientation, since they force polymer to adopt a flow direction as they do not deform and maintain a preferred uniaxial direction by its

natural rigidity. Which sustains the claim that addition of rod-like particles promotes the formation of the nematic phase.

4.4 Structure and morphology – POM

Micrographs in Figures 4.7 and 4.8 show that in fact, there is a nematic phase in the range around 300 ºC. In the first picture at the left, which is the neat matrix, it is seen that there are multiple domains of the nematic phase since different colors can be distinguished. In the case of MWCNT there is also the same behavior as a preferential direction is observed but also formation of some clusters can be identified. It is important to mention that these clusters are seen as dispersed domains. But when HNC are added this multiple domains are interrupted or forced to have the same average direction since there is no more multiple colors, instead there is only one dominant color.

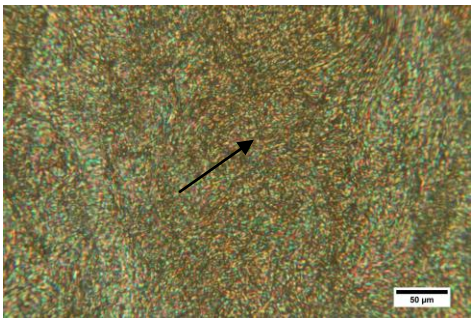

neat

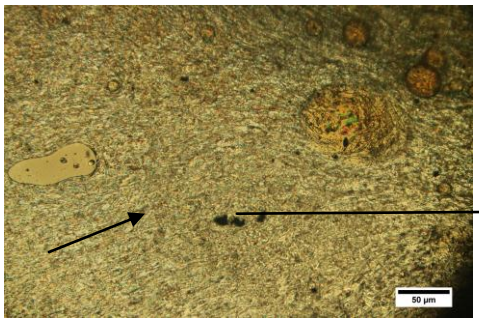

clusters

0.10 v% MWCNT

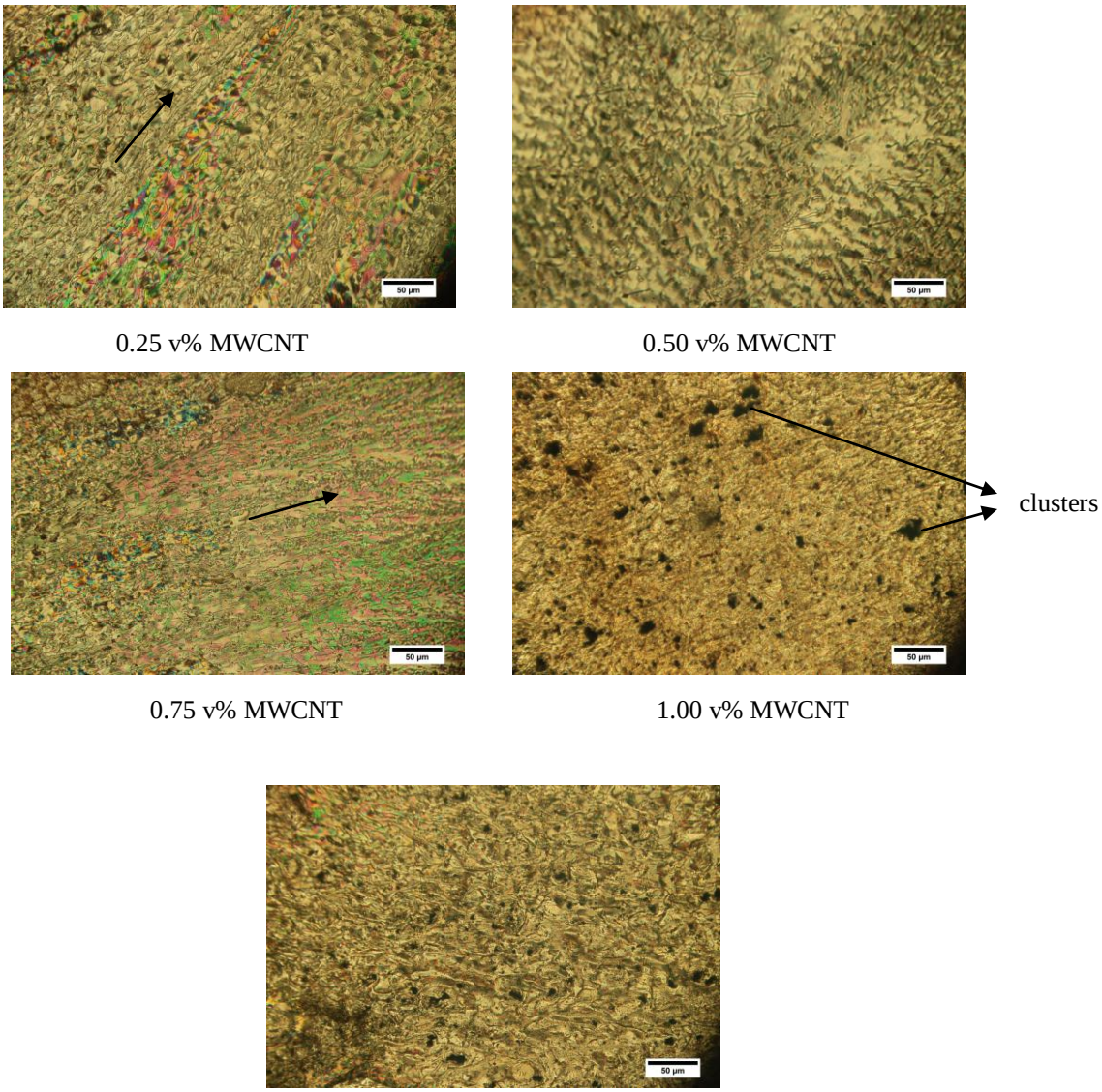

0.25 v% MWCNT

0.50 v% MWCNT

0.75 v% MWCNT

1.00 v% MWCNT

1.50 v% MWCNT

Figure 4.7. Micrographs of PHBA/PET and MWCNT composites.

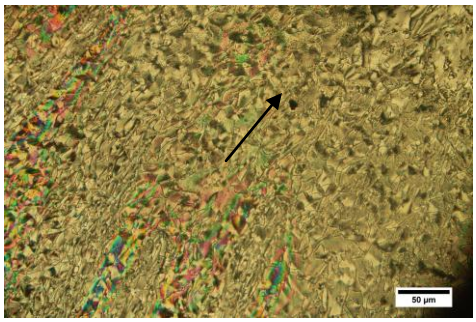

0.10 v% HNC

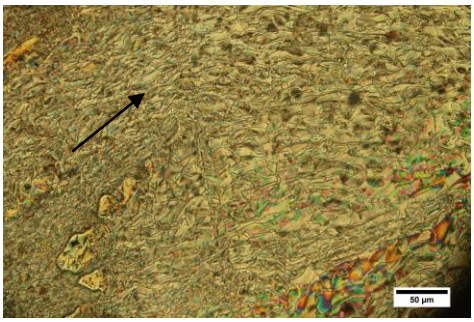

0.25 v% HNC

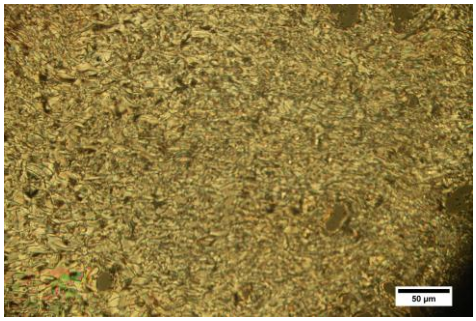

0.50 v% HNC

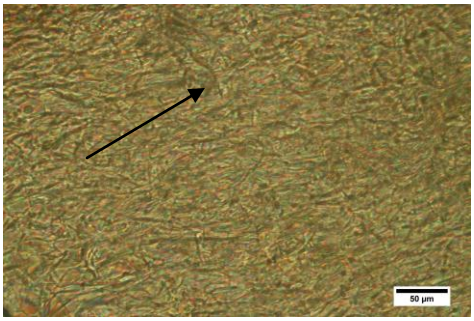

0.75 v% HNC

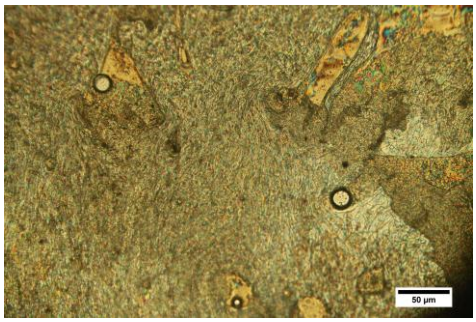

1.00 v% HNC

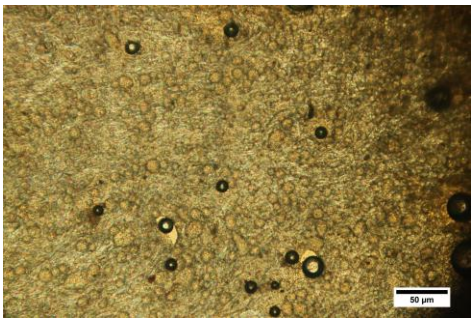

1.50 v% HNC

Figure 4.8. Micrographs of PHBA/PET and HNC composites.

4.5 Structure and morphology – SEM

SEM micrographs of the PHBA/PET – MWCNT system show fibrillar structures at the fracture surface for the complete range of particle loading. These structures are shown in Figure 4.9 and seem to be present as small and distributed clusters, which is characteristic of an aggregated morphology. The formation of these structures is a consequence of good interfacial adhesion due to the functionalized groups on the MWCNT surface, which increases the shearing forces between particle and matrix when stresses are applied. As a result there is a resistance to fracture or crack propagation since the load is transferred from the matrix to the MWCNT through the interface, but when the limit force is reached the composite fails and these reinforcements are broken and/or peeled off, which is what is seen in the micrographs.

The sum of these characteristics, cylindrical morphology and functionalized surface, promote an apparent enhancement in the mechanical properties of the composite since the exerted stress of any load is transferred along the direction of the MWCNT particle and then dispersed within the whole network and small clusters.

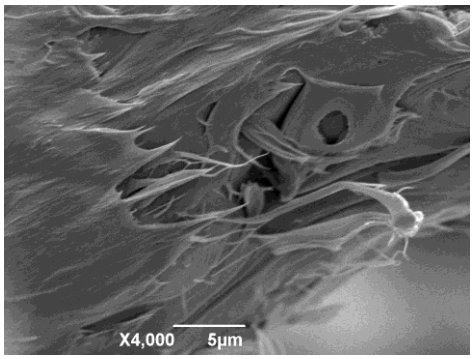

0.10 v% MWCNT

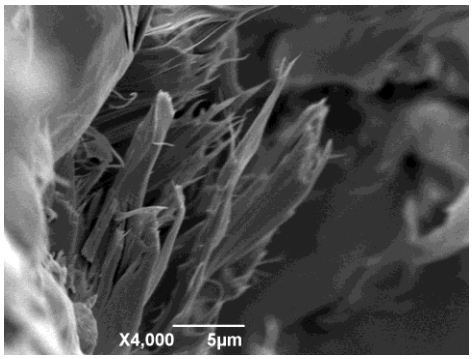

0.25 v% MWCNT

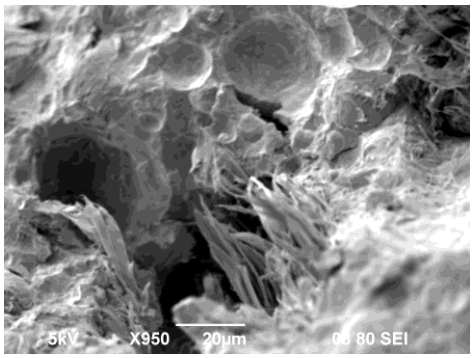

0.50 v% MWCNT

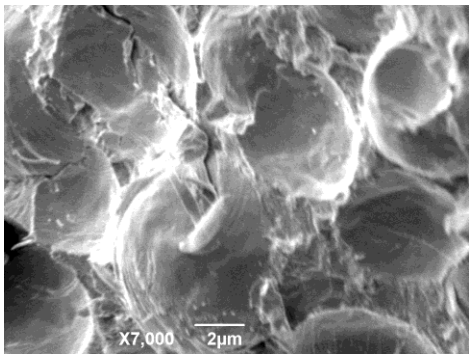

0.75 v% MWCNT

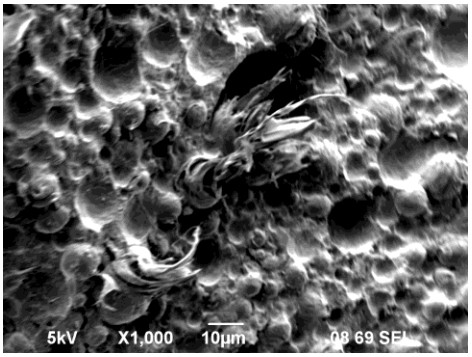

1.00 v% MWCNT

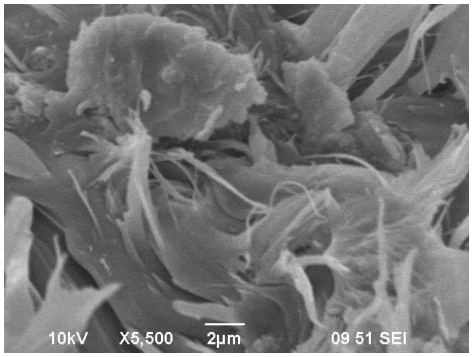

1.50 v% MWCNT

Figure 4.9. Micrographs of PHBA/PET and MWCNT composites.

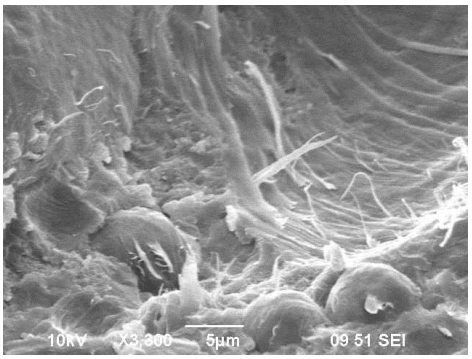

0.10 v% HNC

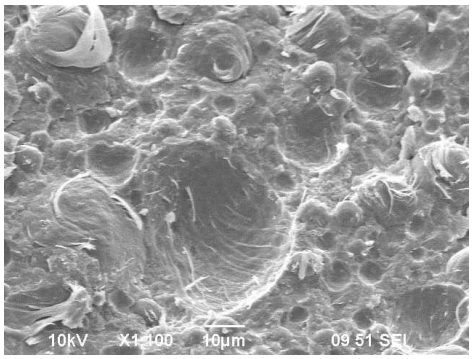

0.25 v% HNC

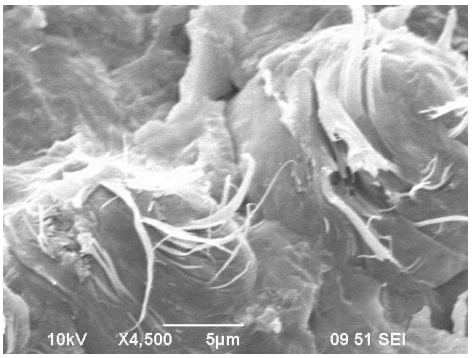

0.50 v% HNC

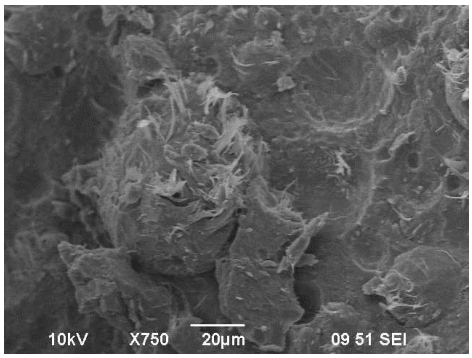

0.75 v% HNC

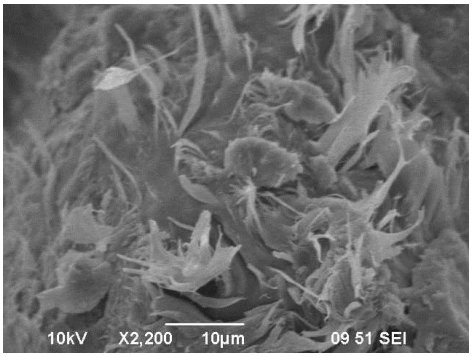

1.00 v% HNC

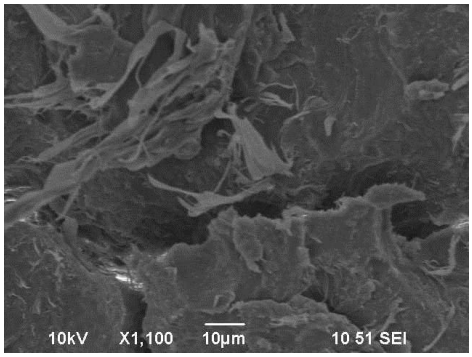

1.50 v% HNC

Figure 4.10. Micrographs of PHBA/PET and HNC composites.

In the case of PHBA/PET-HNC system, there is a rough and fibrillar behavior at the fracture plane surface for all the concentrations studied. This behavior is typical from an intercalated morphology, particle-matrix arrangement, rather than an aggregated one, such as in the PHBA/PET-MWCNT system. The formation of this intercalated morphology is promoted by the HNC galleries which tend to sandwich the matrix molecules. While the fibrillar behavior is a result of particles being pulled off from the matrix, as shown in Figure 4.10.

4.6 Structure and morphology – SAXS

Small angle X-ray patterns were recorded in order to study the effect of cylindrical shaped nanoparticles (i.e. MWCNT and HNC) on the LC structure of the matrix. As shown in Figure 4.11 and Figure 4.12, there are no significant changes on the intensities of both curves. The only difference is that HNC curve has a slight higher hump than the MWCNT curve, which may be related to the presence of more intercalated structures when compared to the MWCNT system.

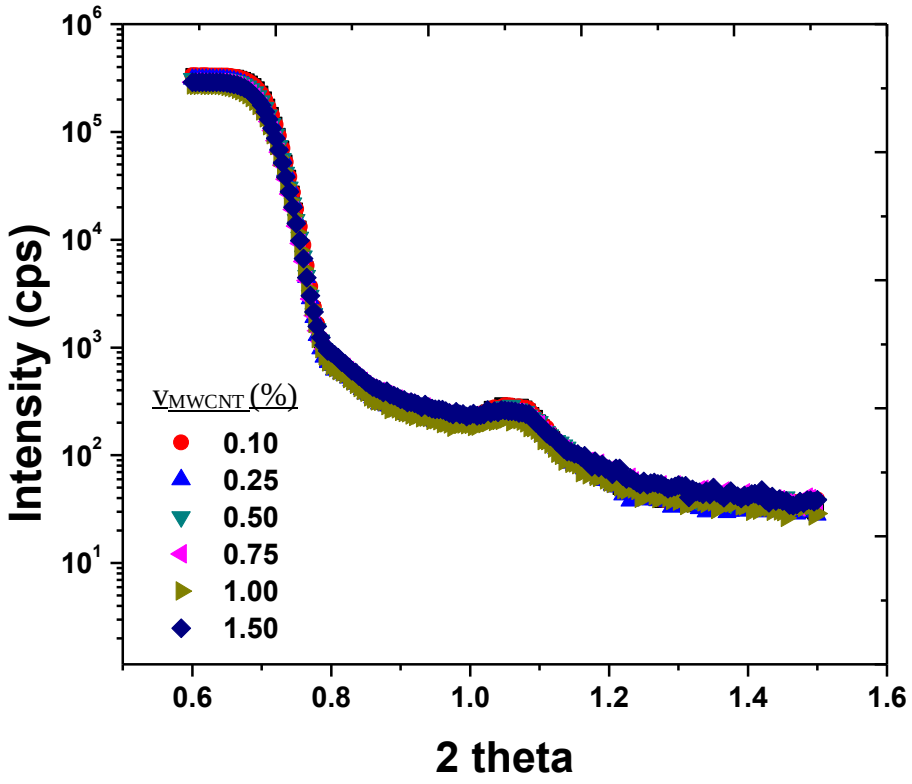

Figure 4.11. Effect of MWCNT particles on the SAXS patterns of PHBA/PET comoposites.

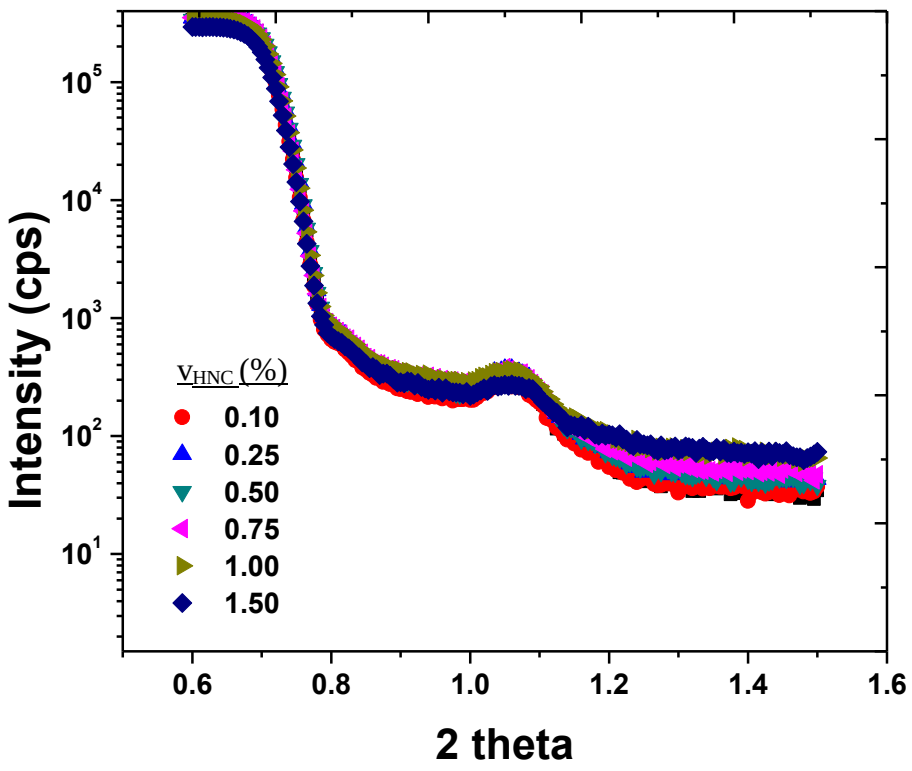

Figure 4.12. Effect of HNC particles on the SAXS patterns of PHBA/PET comoposites.

Cylindrically shaped particles does not change or significantly affect the structure of the matrix since they are oriented in the same direction of the matrix molecules as a result of the extrusion process, which forces a preferential direction but it does improves the percentage of LC domains.

4.7 Conclusion

From the studies performed halloysite nanoclay seems to have a better performance than multiwalled carbon nanotubes when enhancing composite resistance to thermal degradation. More than that, MWCNT does not significantly improve the thermal properties of PHBA/PET. Instead of increasing the degradation temperatures, addition of MWCNT promoted faster degradation in some cases such as in T_5, T_{10} and T_{md1}.

Addition of rod-like nanoparticles lowered the energy requirement for reaching the glass transition and less energy liberation at the isotropic-to-nematic transition. This is attributed to an increment in volume between polymer molecules for the glass transition and evidence of more oriented structures at the isotropic to nematic transition. This orientation is enhanced due to particle morphology which will add rigidity and restrict or limit molecular misalignment. The major effect in energy reduction is observed with the MWCNT particles. This behavior may be attributed to the higher rigidity of MWCNT which will give a more ordered structure. For both particles the heat of fussion (ΔH_m) is increased since at this point the sample components (matrix and particles) will require energy in order to flow freely.

The presence of nematic structures is confirmed with the POM technique at the range around the 300 ºC. Also some multiple domains are observed at low

concentrations of HNC but disappear as concentration increases, which may be attributed to more orientation. In the case of MWCNT some clusters are seen at different concentrations, which is evidence of a poor dispersion.

Rod-like particles promote the formation of fibrillar structures as shown by the SEM micrographs which is related to possible mechanical enhancement since it could represent a resistance to fracture or composite failure. HNC composites show a more intercalated behavior since a more fibrillated surface at fracture plane is observed.

To summarize, rod-like reinforcements could promote mechanical improvements, but to confirm this more exhaustive mechanical tests need to be performed. In addition, no significant change in the liquid crystalline structure is observed for either MWCNT or HNC. While HNC seems to promote better thermal enhancement than MWCNT and both nanoparticles reduce the liquid crystalline range.

5. EFFECT OF SPHERICAL SHAPED PARTICLE ON THE STRUCTURE AND THERMAL PROPERTIES OF THERMOTROPIC LIQUID CRYSTALLINE POLYMER NANOCOMPOSITES

5.1 Introduction

Polymer composites have been studied in the last few decades for a wide variety of engineering applications [96-98]. Recently the interest has been focused on systems where filler size lie in the nanometer scale, or nanocomposites [99]. Great improvements on the mechanical and thermal properties, when compared to the neat matrix, have been demonstrated with just minute ammounts of nanoparticles [100, 101]. The improvements in the physical and chemical properties are primarly due to the large surface area per unit volume of the fillers, which allow for enhanced interactions with the matrix molecules.

Liquid crystalline polymers are composed of linear semi-rigid molecules which are capable of forming oriented or anisotropic structures. Specifically polymers that show nematic structures are very attractive for polymer processing techniques such as extrusion, since they have low melt viscosity and can be easily oriented in the flow direction [102]. The interest in studying these systems resides in the potential

possibility of producing ligthweight components, while promoting excellent mechanical and thermal performance at lower production costs [103].

In this kind of composites, the formation of fibrillar structures is related to composite property enhancement. While structures such as those reported by Quin [104], where ellipsoids and short fibrils were found on Rodrun LC 3000/PP composites, does not promote relevant property improvements. In this chapter the effect of spherical silica nanoparticles inclusion, at loadings up to 1.5 v%, on the thermal transitions and structure of model thermotropic matrix 60:40 mol% poly(4-benzoic acid-co-ethylene terephthalate) (PHBA/PET) uniaxial film nanocomposites produced by direct melt blending on a twin screw extruder was studied.

5.2 Thermal characterization – TGA

As mentioned before, PHBA/PET degrades in two stages corresponding to each of its monomeric units, as shown in Figure 5.1.

From the thermogravimetric analysis curves it can be deduced that the addition of silica nanoparticles improve composite thermal stability, since there is a displacement on the degradation stages toward higher temperatures when silica particles are added.

A displacement toward higher values is observed in both cases. This may be attributed to the formation of hydrogen bonds beteween the SiO_2 and the carboxyl

groups of the PHBA and PET units. This interfacial affinity between particle and matrix molecules may improve the thermal properties of the composites.

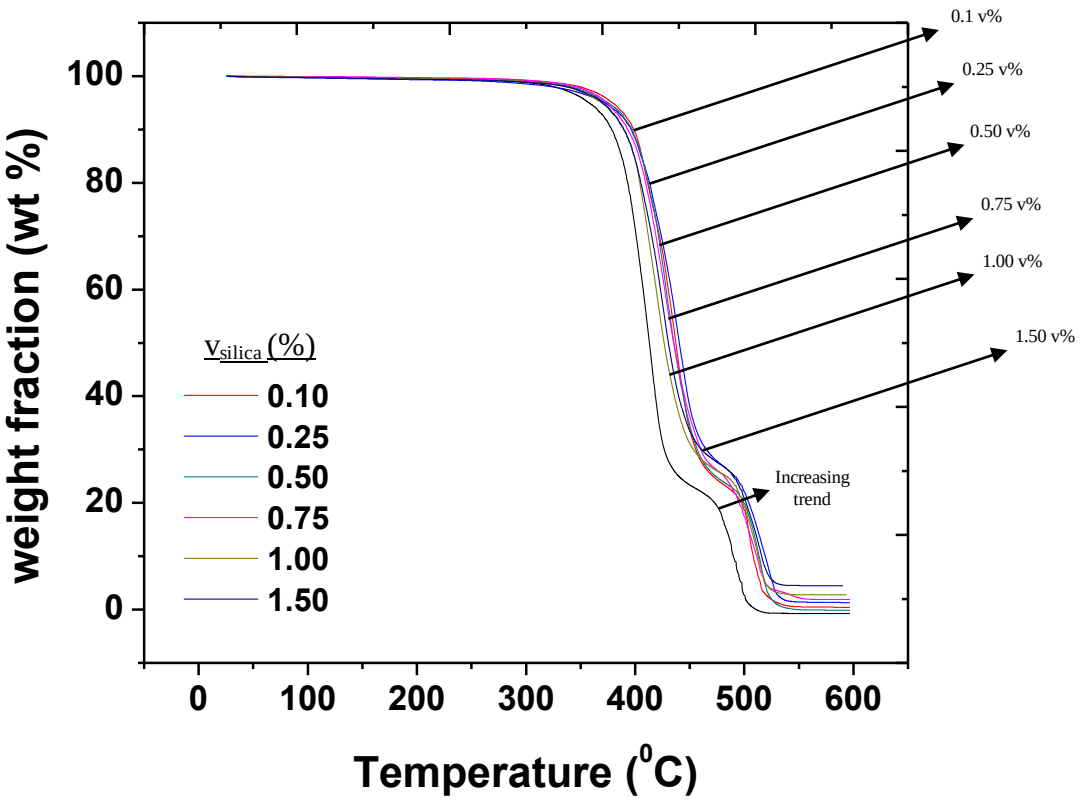

Figure 5.1. Thermogravimetric characterization of PHBA/PET and silica nanocomposites.

Table 5.1. Effect of silica fillers on the thermal stability of the PHBA/PET nanocomposite.

Silica (v%)	T_5 [a] (°C)	T_{10} [b] (°C)	$T_{md\ 1}$ [c] (°C)	$T_{md\ 2}$ [d] (°C)
Neat	357.6	378.2	412.2	490.5
0.1	379.3	398.8	435.8	504.0
0.25	372.3	396.5	438.8	519.9
0.5	375.3	397.3	426.8	512.1
0.75	374.2	393.3	424.4	509.4
1.0	369.6	389.5	422.1	516.8
1.5	370	389.6	431.3	520.2

a - Temperature at a weight loss of 5 % b - Temperature at a weight loss of 10 %
c - Temperature at 1st maximum of 1st derivative d - Temperature at 2nd maximum of 1st derivative

Table 5.1 summarizes the degradation temperatures at 5 and 10 weight loss as well as at the two maximum degradation rate stages. As it is seen, at weight loss of 5 and 10 % temperatures are displaced by an average of 15.85 and 15.97 ºC respectively. While the first stage of degradation is increased by an average of 17.67 ºC. For the second degradation stage, temperature is increased by an average of 23.23 ºC. This suggests a thermal property enhancement as the composite degradation is being delayed to higher values which could be of important use for different applications were high temperature resistant components are needed. Also, it can be observed that temperatures does not change significantly by varying concentration, which means that

with relatively low concentrations similar enhancements can be achieved, which is of great importance economically speaking and from a material production point of view. This behavior was consistent at all the studied degradation temperatures.

5.3 Thermal characterization – DSC

DSC thermograms for the neat PHBA/PET matrix and composites, shown in Figure 5.2, show three thermal transitions. The first transition appears around the 50 °C and is identified as the glass transition (T_g). The second transition is around 180 °C and corresponds to the melting of crystallites (T_m). Finally above the 300 °C, the temperature reaches a maximum peak, identified as the characteristic temperature for the isotropic-to-nematic phase transition (T_{IN}). The transition temperatures for the polymer matrix and nanocomposites are summarized in Table 5.2. The characteristic temperatures for these transitions were obtained using the Universal Analysis software by taking the minimum peak temperature for the endothermic glass and melting transitions, and the maximum peak temperature of the exothermic isotropic-to-nematic transition.

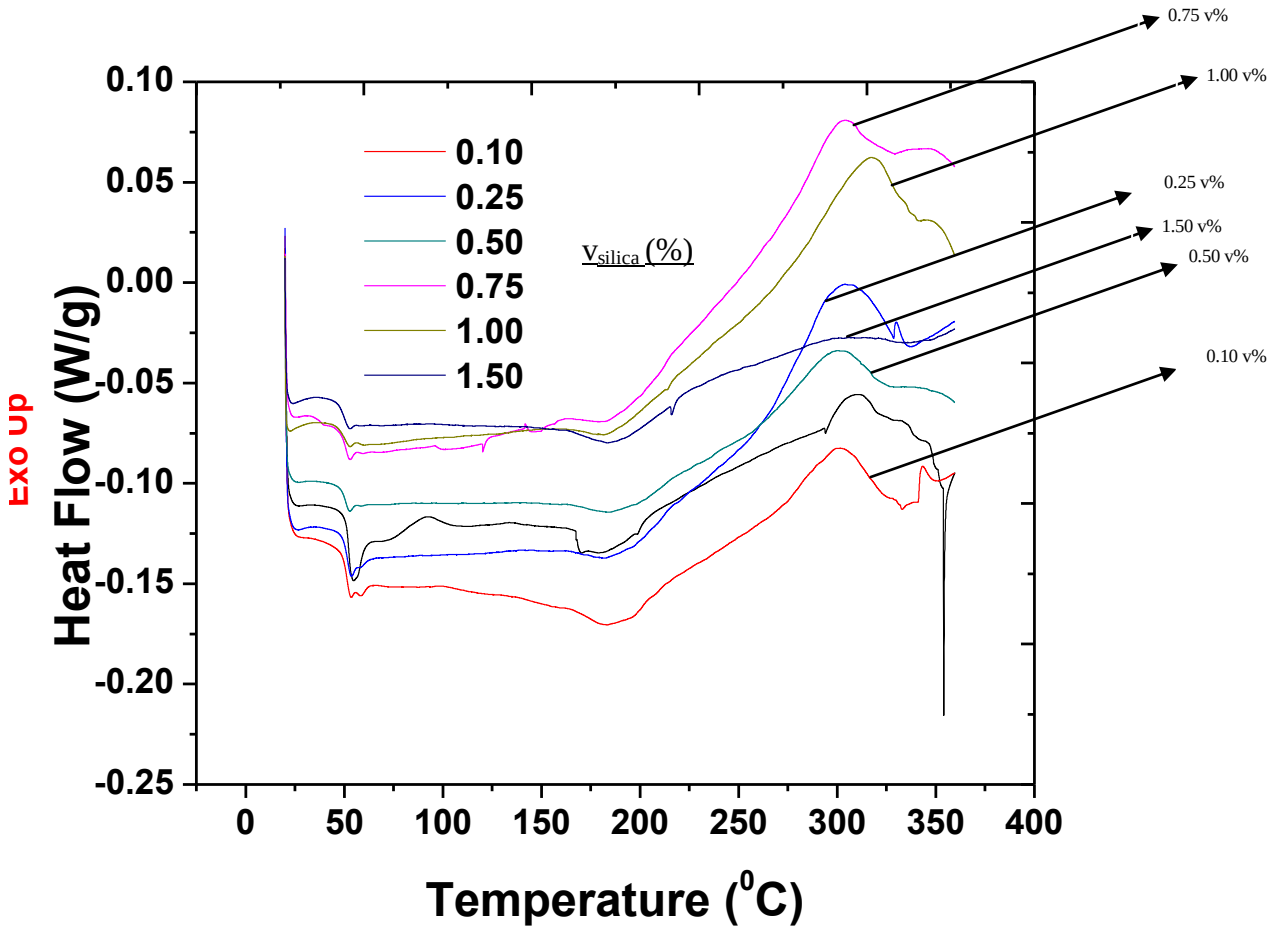

Figure 5.2. DSC thermograms of PHBA/PET silica nanocomposites.

Table 5.2. Effect of silica fillers on the transition temperatures of the PHBA/PET nanocomposite.

Silica (v %)	T_g * (°C)	T_m * (°C)	T_{IN} * (°C)
Neat	52.2	184.2	330.0
0.10	53.0	182.4	302.3
0.25	53.5	186.8	301.8
0.50	52.5	198.2	300.9
0.75	52.4	192.4	304.1
1.00	54.8	193.0	307.0
1.50	51.3	185.2	302.0

T_g – glass transition T_m – melting point T_{IN} – isotropic to nematic phase

*Average values taken from a total of n=3 measurements.

Addition of silica nanoparticles does not have a significant effect on the glass transition temperature since it remains almost constant, this behavior can also be seen in Figure 7.1. While the melting point shows an increment from medium to high concentrations (0.5 – 1.0 v%), which may be attributed to the interactions between the polymer chains and the nanoparticles and to the reduction of macromolecular chain mobility around the nanoparticles, but as shown in Figure 7.1, the values may lie in the error region. On the other hand, the temperature range, where the liquid crystalline phase lies seems to be supresed as the peak temperature (at nematic phase) decreases

from 330 °C for the neat matrix to values ranging from 300 to 307 °C, independently of loading. Again, values lie in the error region which could mean that no significant changes are promoted.

Table 5.3. Transition enthalipies for PHBA/PET silica composites.

Silica (v %)	ΔH_g * (J/g)	ΔH_m * (J/g)	ΔH_{IN} * (J/g)
Neat	1.01	3.54	1.25
0.10	1.17	2.40	11.12
0.25	1.29	1.78	19.12
0.50	0.447	4.35	12.22
0.75	0.590	3.59	12.89
1.00	0.311	2.89	12.74
1.50	0.495	1.94	12.48

ΔH_g – glass transition ΔH_m – melting point ΔH_{IN} – isotropic to nematic phase

*Average values taken from a total of n=3 measurements.

Comparing the transition enthalpies, summarized in Table 5.3, determined as the area under the curve obtained using the Universal Analysis software of TA Instruments, it can be deduced that addition of silica nanoparticles lowers the enthalpy of the glass transition. This may be attributed to the imperfections caused by the

particles on the semicrystalline lattice of the matrix, which increases the volume between polymer molecules. The latter translate into a lower energy requirement in order to pass from a solid state to a more relaxed system, since some disorder has been introduced to the system by the spherical fillers. This effect is more evident as particle concentration was increased, but at lower particle loadings (i.e. 0.1 & 0.25 v%) thermal stability was promoted.

The heat of fusion (i.e. enthalpy at the melting point) does not show a trend with the addition of silica. Reproducibility values in Figure 7.2 show that the heat of fusion diminishes from 0.1 v% to 0.5 v% but increases from 0.75 v% to 1.5 v%. For the enthalpy associated with nematic phase transition a significant change, at least a factor of 10, was observed as the amount of silica increases. This behavior can also be seen in Figure 7.2. A higher attraction between the silica surface and the polymer distorts the liquid crystalline ordering, but remaining nematic regions may be confined between particle agglomerates. This behavior deviates from the rod-like nanoparticles since this time more energy is being liberated at the isotropic to nematic transition.

5.4 Structure and morphology – POM

POM confirmed nematic ordering of the composites within the range determined by DSC. Figure 5.4 shows sample micrographs of the neat polymer and some silica nanocomposites around the 300 °C. The reported photos were taken at the approximate range where the nematic-to-isotropic phase transition peak is observed using the DSC technique. Furthermore, there was neither significant change as particle concentration increased nor evidence of particle percolation. Yet, the formation of multiple spherulites is evident, which may be attributed to the silica acting as a nucleating agent. In this melt state the deformation of molecules near particle surface is known to show this behavior [92].

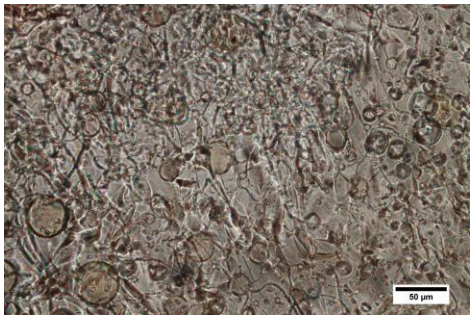

neat

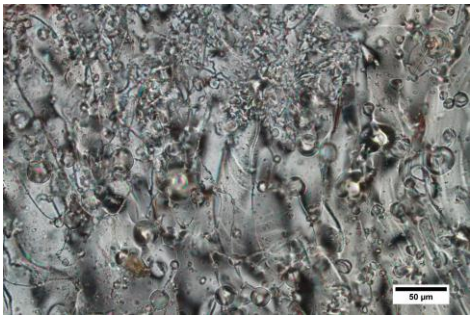

0.10 v% silica

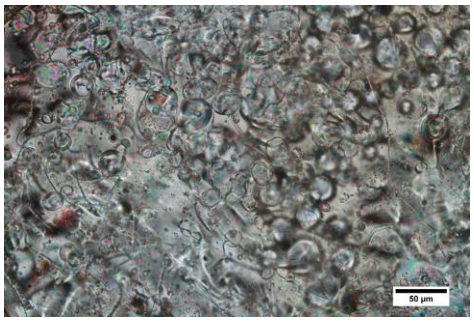

0.25 v% silica

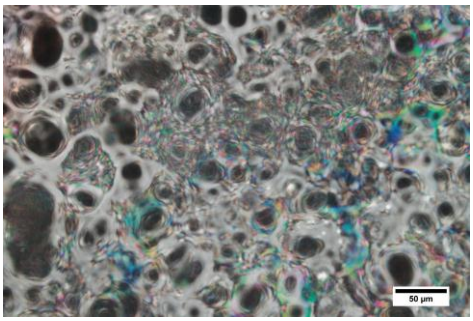

0.50 v% silica

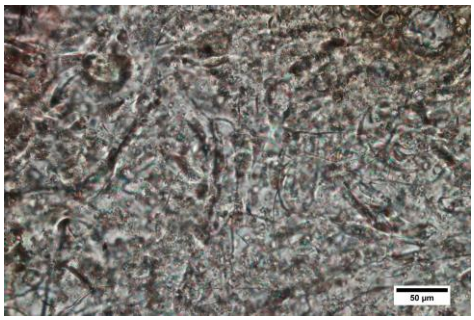

0.75 v% silica

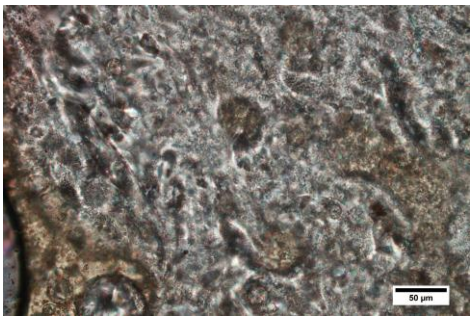

1.00 v% silica

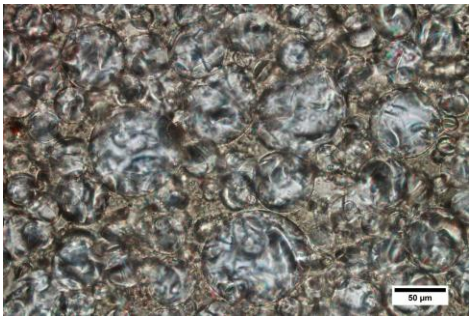

1.50 v% silica

Figure 5.4. Micrographs of PHBA/PET and silica composites.

5.5 Structure and morphology – SEM

Another analysis performed on the composite was the study of the fracture planes by SEM, as shown in Figure 5.5. No fibrillar surfaces were identified; this is attributed to the spherical morphology of the particles which does not promote preferential orientation over the polymer molecules. Instead, the formation of circular structures (voids) and a smooth film surface were observed. These types of structures are related to poor mechanical properties, since the particles do not provide resistance to failure or crack propagation.

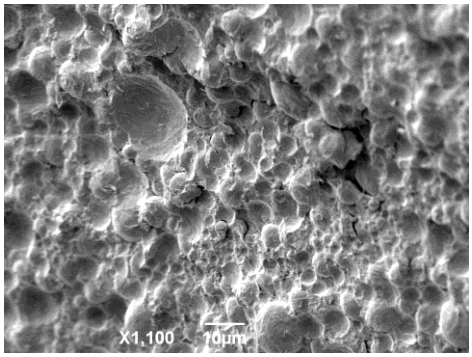

0.10 v% silica

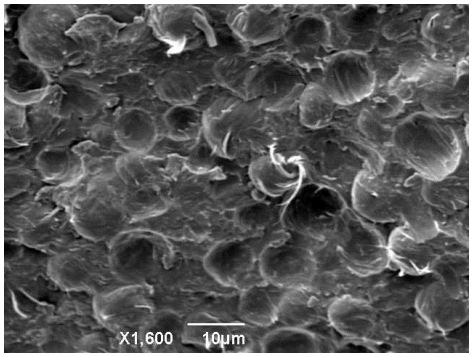

0.25 v% silica

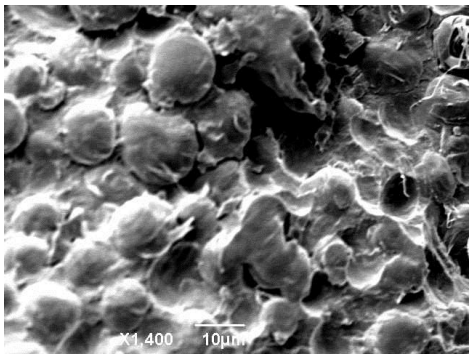

0.50 v% silica

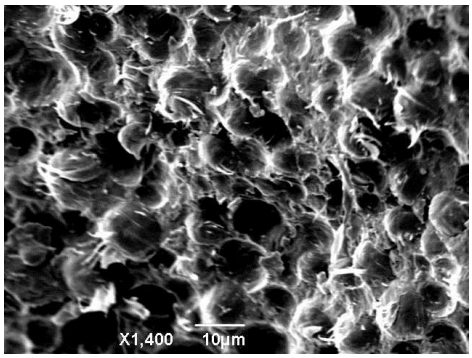

0.75 v% silica

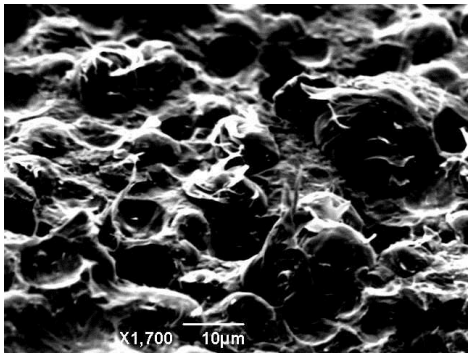

1.00 v% silica

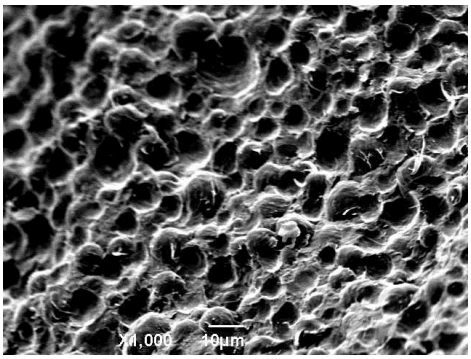

1.50 v% silica

Figure 5.5. Micrographs of PHBA/PET and silica composites.

5.6 Structure and morphology – SAXS

SAXS difractograms are shown in Figure 5.6. No differnce in peak position was observed within the studied particle loading range. Thus, no change in the LC ordering is promoted by the silica nanoparticles. Yet, the small changes in intensity might suggest an increment in the ammount of crystal domains distribution.

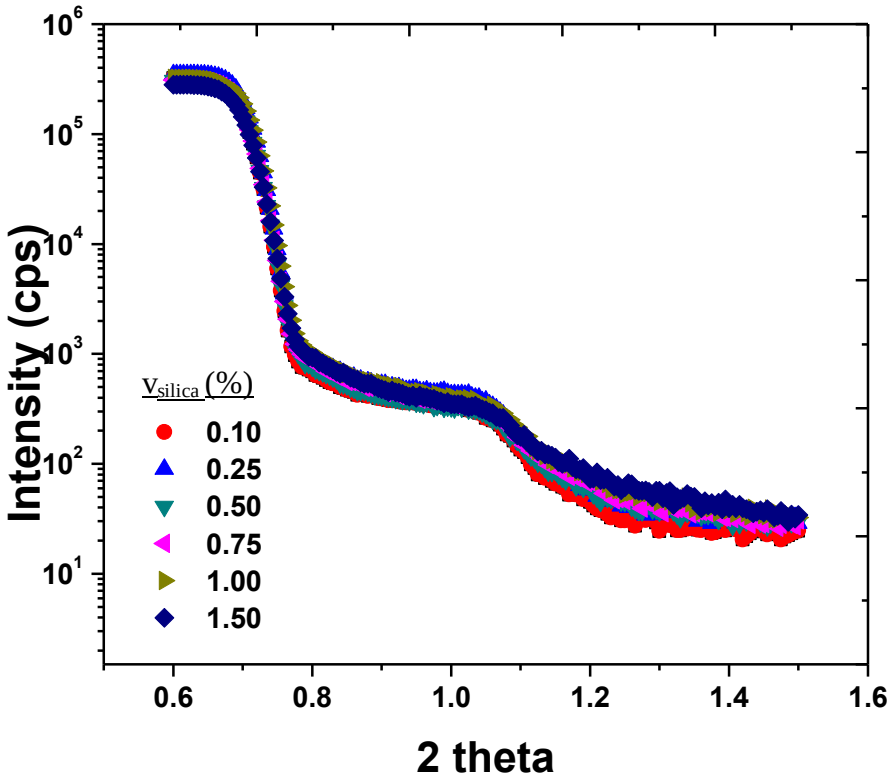

Figure 5.6. Effect of silica particles on the SAXS patterns of PHBA/PET comoposites.

5.7 Conclusion

Addition of silica nanoparticles significantly enhances composite thermal properties, especially at low amounts of particle loading. All degradation temperatures studied were increased by at least 10 ºC but the most significant values were obtained at 0.1 and 0.25 v% of concentration. This result may be very attractive to those applications were components with high temperature resistance need to be produced without sacrificing or also improving other parameters such as weight.

In the case of transition temperatures silica does not significantly affect the values at which glass and melting point are reached. This could be an effect of particle morphology since a spherical shape does not promote a preferential orientation. The only effect that addition of these particles will cause is an increment in the volume and/or space between polymer molecules without disturbing their deformation. While for the isotropic to nematic transition a significant decrease is observed when silica is added. But temperatures remain almost constant, with just little variations as function of particle loading. This cannot be confused with liquid crystalline phase promotion, instead this may be attributed to the thermal properties of silica, which are dispersed in a nematic phase acting as efficient temperature delayers.

The energy at glass and melt transitions decreases when comparing the different concentrations with the neat matrix, the reason why this occurs was explained in

Chapter 3 and 4. Since there is a disturbance on the molecular ordering induced by the spherical particles who do not promote a preferential orientation; polymer molecules now need to liberate more energy in order to reach an equilibrium state of orientation.

The formation of dispersed spherulites is observed in some of the POM micrographs. But no significant difference is observed in the nematic phases as particle concentration changes. While for the SEM micrographs no fibrillar structures were observed at the fracture plane which could be related to poor mechanical properties, but further tests need to be performed in order to conclude this. Liquid crystalline phase range was diminished as T_{IN} was reduced while T_m did not had a significan change. While SAXS patterns show that a possible increment in the crystal distribution domains could be a reason for the widened curve/peak shape.

6. EFFECT OF PLATELLET SHAPED PARTICLE ON THE STRUCTURE AND THERMAL PROPERTIES OF THERMOTROPIC LIQUID CRYSTALLINE POLYMER NANOCOMPOSITES

6.1 Introduction

Polymer clay nanocomposites have attracted great attention since with a small addition of particles they offer a large interfacial area which gives them many properties such as: increased mechanical properties, gas permeability and fire retardant properties among others [105]. Mechanical property enhancement is related to the formation of fibrilar structures and type of dispersion [106], while thermal/fire retardant properties are related to a barrier formed by clays galleries which act as a labyrinth impeding or delaying the mass transport of degrading polymer species.

Addition of MNC showed to improve matrix thermal stability as the degradation temperatures studied (T_5, T_{10}, T_{md1} & T_{md2}) where displaced to higher values as particle concentration increased. DSC analysis showed that glass temperature does not seem to be affected since temperature values remained almost constant. While for the melting point, particle concentration showed an effect at concentrations higher than 0.5 v% as temperature values started to decrease. In the case of isotropic-to-nematic transition a decreasing trend can be identified.

Liquid crystalline phases were identified at the different concentrations studied, demonstrating that MNC does not affect liquid crystallinity. Fibrillar structures are observed in the SEM micrographs, which are related to possible mechanical enhancement. Also, internal structure of composite was studied using SAXS, where the intensities increased almost as a function of particle volume.

6.2 Thermal characterization – TGA

Thermogravimetric analysis was performed on the MNC composites to study their effect as particle concentration varied. Figure 6.1 shows the TGA curves for the different composite loadings.

From Figure 6.1 it is seen that addition of MNC systematically increases composite degradation resistance as a function of concentration. Addition of MNC improves thermal stability of composites since T_5 has an average increment of 15.68 ºC while T_{10} increases by an average of 14.67 ºC as it can be seen from Table 6.1. The temperatures that define the two major degradation stages, T_{md1} and T_{md2}, are displaced by an average of 12.85 ºC and 36.53 ºC, respectively. This temperature resistance is a great advantage that could be exploited in a wide variety of applications since the composite can be exposed to a more hostile and high temperature environment than the neat matrix. The thermal enhancement is a consequence of the montmorillonite gallery

structure which helps in the deviation of heat through them instead of going exclusively through the matrix.

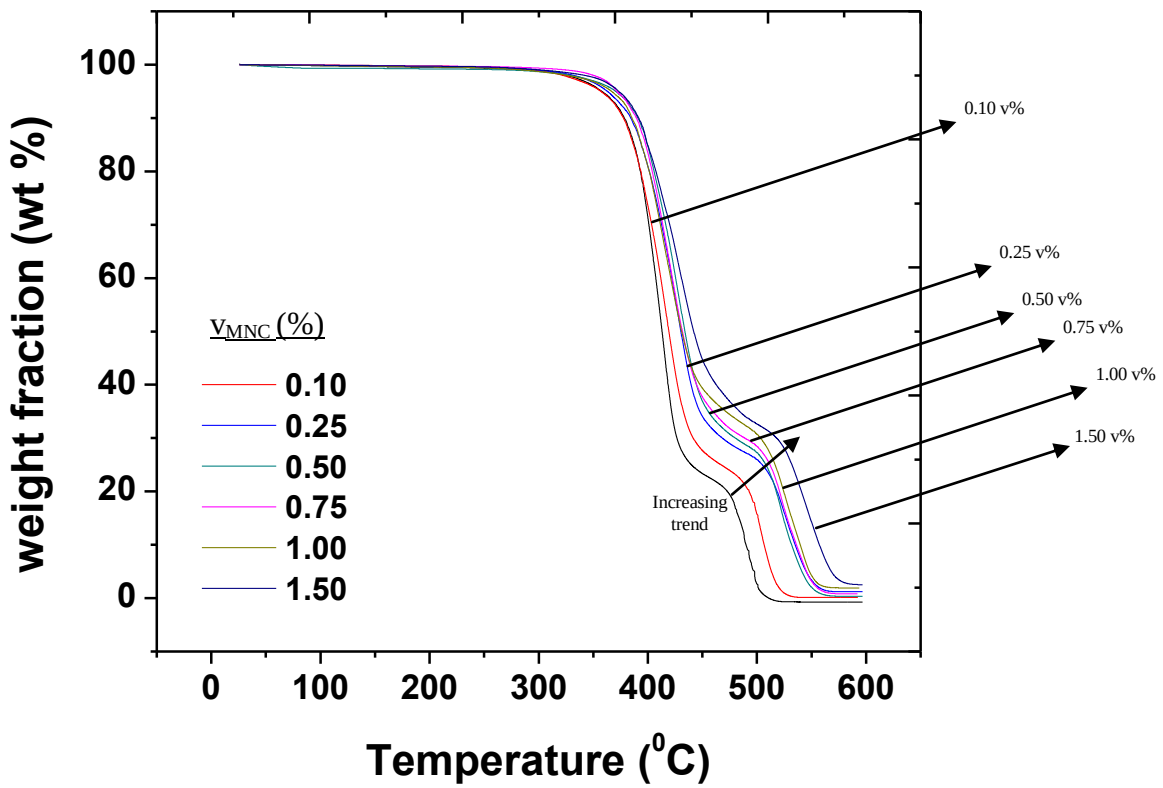

Figure 6.1. Thermogravimetric characterization of PHBA/PET and MNC nanocomposites.

Table 6.1. Effect of MNC fillers on the thermal stability of the PHBA/PET nanocomposite.

MNC (v%)	T_5 [a] (°C)	T_{10} [b] (°C)	$T_{md\ 1}$ [c] (°C)	$T_{md\ 2}$ [d] (°C)
Neat	357.6	378.2	412.2	490.5
0.10	363.3	383.9	422.8	511.4
0.25	369.2	390.7	428.7	527.5
0.50	376.8	397.1	426.0	520.1
0.75	377.8	395.8	424.6	527.5
1.00	373.0	391.7	419.7	529.0
1.50	379.6	398.0	428.5	546.7

a - Temperature at a weight loss of 5 % b - Temperature at a weight loss of 10 %
c - Temperature at 1st maximum of 1st derivative d - Temperature at 2nd maximum of 1st derivative

6.3 Thermal characterization – DSC

Composite thermal transitions were studied by obtaining the characteristic temperatures and enthalpies of each transition. Figure 6.2 shows the thermal behavior of MNC composites at different concentrations, but the specific values of temperature and enthalpy for each phase are collected on Table 6.2 and Table 6.3 respectively.

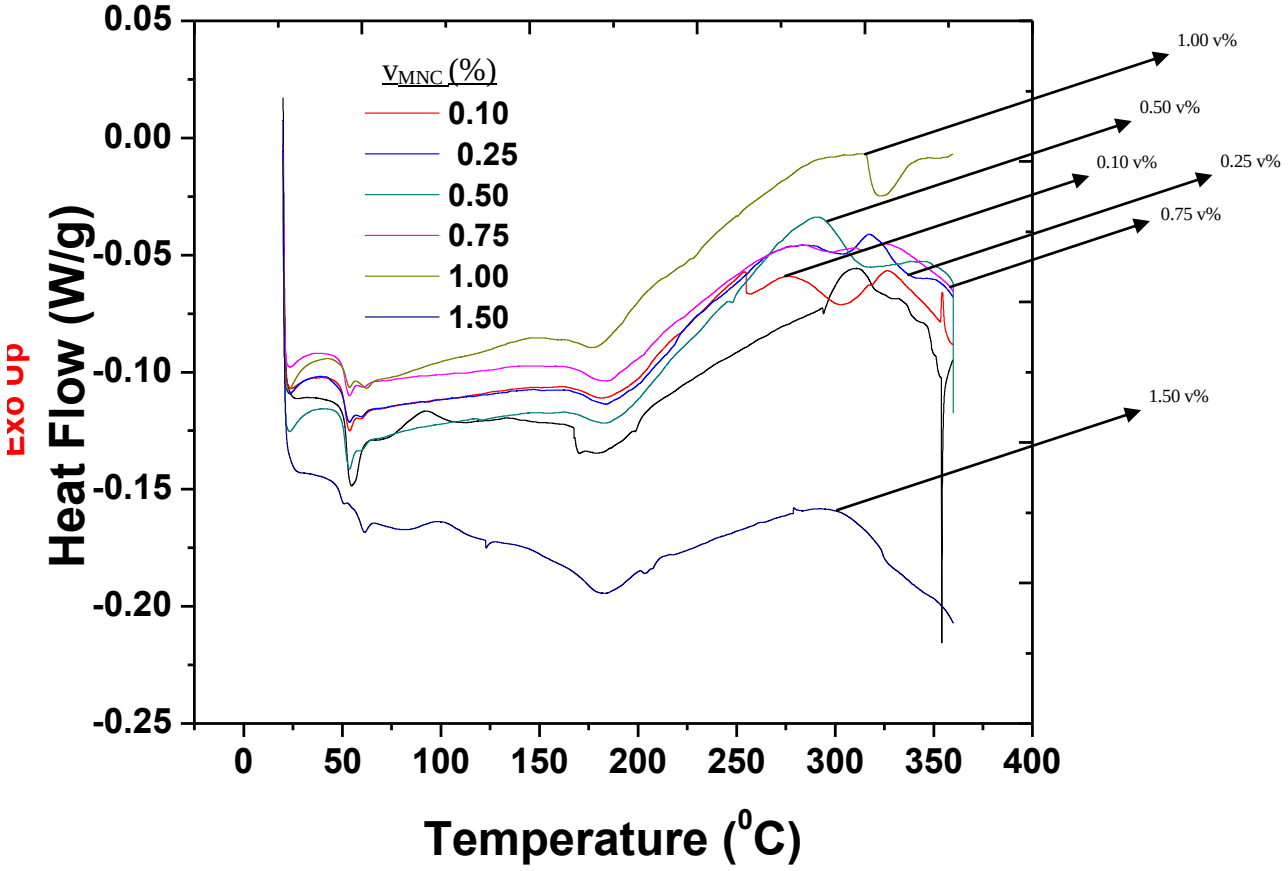

Figure 6.2. DSC thermograms of PHBA/PET MNC nanocomposites.

The glass transition temperature remained almost constant; increments of just 2 ºC were observed for some of the concentrations. Glass temperature values have small deviations (~3 ºC) as shown in Figure 7.1 may lie within the error range. The later

implies that polymer molecules may be exfoliated between the platellete-like particles since their addition does not represent or induces a significant change in intermolecular (specific) volume. In the case of melting point interestingly temperature values are reduced. But looking at the Figure 7.1 the melt temperature values have relatively small variations and it can be stated that the values remain almost inside the same temperature range for low to medium concentrations. But for concentrations higher than 0.5 v% temperature values drop. This is an advantage from the processing point of view since energy is saved. But may be a negative effect for some applications since composite will melt easily. This behavior may imply that the effect of MNC partile loading as a thermal property enhancer is more effective as particle concentration is increased. On the other hand, the isotropic-to-nematic characteristic temperature is also decreased by an average amount of 54.7 ºC. This means that the isotropic phase can be reached at lower temperatures with increasing MNC concentration. For low to medium concentrations temperature values remain almost in the same values while at concentartions from 0.75 v% to 1.5 v%, temperature values drop considerably.

Table 6.2. Effect of MNC fillers on the transition temperatures of the PHBA/PET nanocomposite.

MNC (v %)	T_g * (°C)	T_m * (°C)	T_{IN} * (°C)
Neat	52.2	184.2	330
0.10	53.5	178.8	297.6
0.25	54.9	171.4	287.8
0.50	53.0	177.7	291.9
0.75	53.7	158.6	252.0
1.00	53.6	156.1	264.1
1.50	54.6	166.3	258.3

T_g – glass transition T_m – melting point T_{IN} – isotropic to nematic phase

*Average values taken from a total of n=3 measurements.

Table 6.3. Transition enthalipies for PHBA/PET MNC composites.

MNC (v %)	ΔH_g * (J/g)	ΔH_m * (J/g)	ΔH_{IN} * (J/g)
Neat	1.01	3.54	1.25
0.10	0.929	2.79	4.35
0.25	1.60	1.21	5.49
0.50	0.656	10.7	0.927
0.75	0.792	0.564	0.866
1.00	1.17	0.623	4.40
1.50	1.24	4.66	6.33

ΔH_g – glass transition ΔH_m – melting point ΔH_{IN} – isotropic to nematic phase

*Average values taken from a total of n=3 measurements.

The energies for each transition have a random behavior but a decreasing behavior can be identified as shown in Figure 7.2. Less energy is required in order to promote a change in volume. Melt transition energies show a trend of lowering as particle concentration increases except for the 1.5 v%. Initial values reamain within the error range.

6.4 Structure and morphology – POM

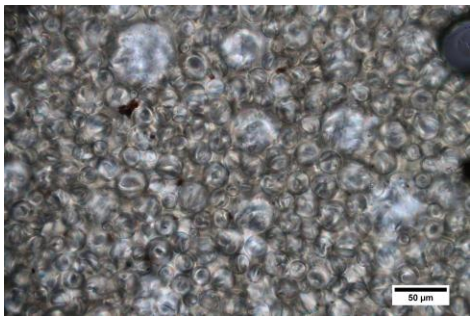

0.10 v% MNC

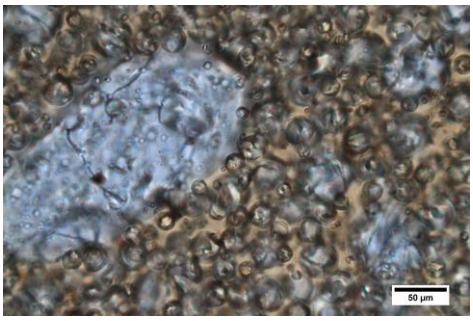

0.25 v% MNC

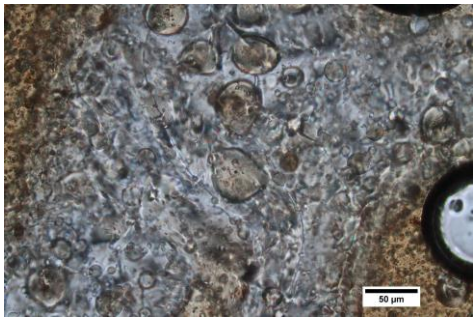

0.50 v% MNC

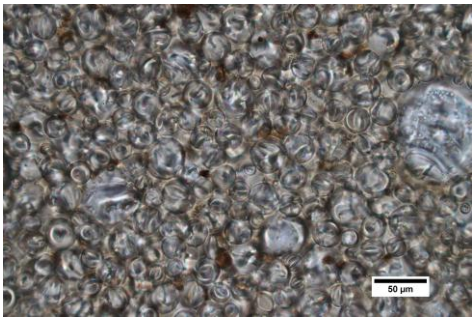

0.75 v% MNC

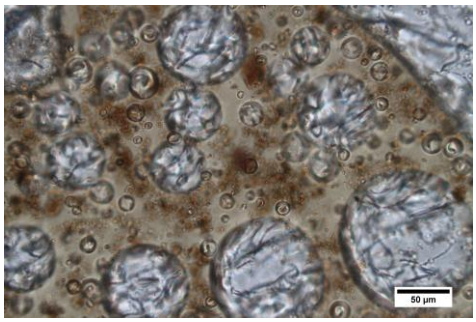

1.00 v% MNC

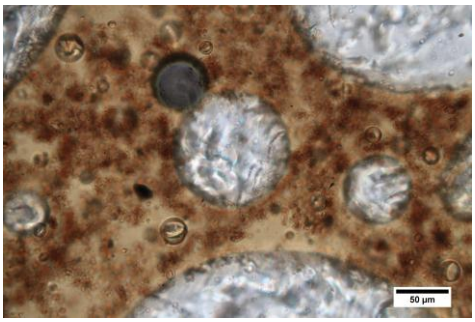

1.50 v% MNC

Figure 6.3. Micrographs of PHBA/PET and MNC composites.

The technique of POM microscopy was used to confirm the presence of the nematic phase at the range of 300 ºC previously identified with the DSC technique. Figure 6.3 shows the micrographs for the MNC composites micrographs where nematic structures can be identified as well as the appearance of multiple spherulites which implies good particle dispersion or the presence of exfoliated structures.

6.5 Structure and morphology – SEM

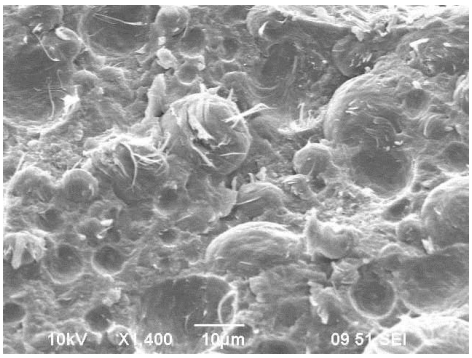

0.10 v% MNC

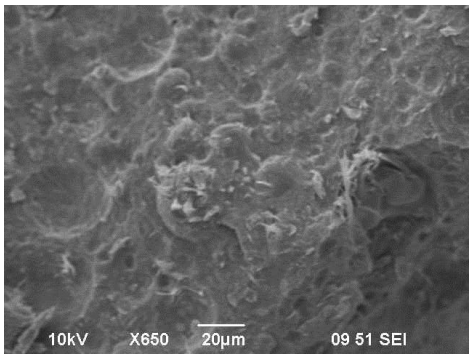

0.25 v% MNC

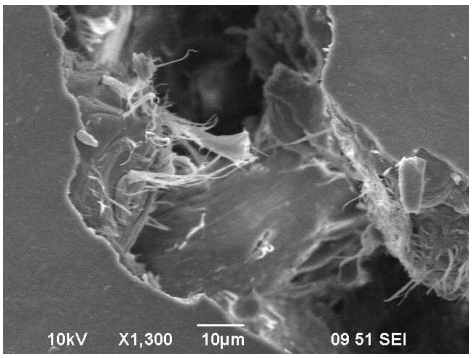

0.50 v% MNC

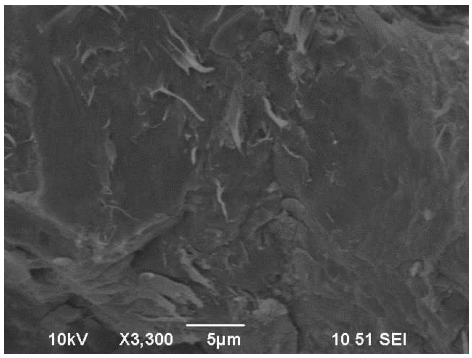

0.75 v% MNC

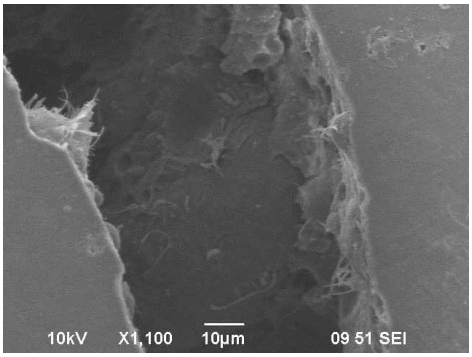

1.00 v% MNC

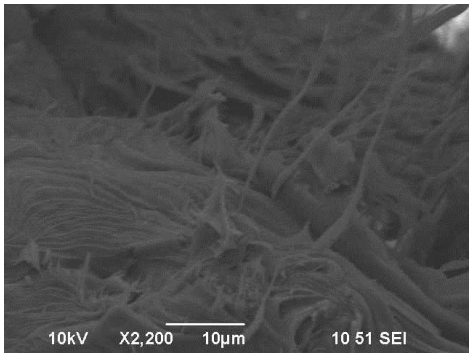

1.50 v% MNC

Figure 6.4. Micrographs of PHBA/PET and MNC composites.

SEM micrographs show a fibrillar behavior at the fracture plane for all the studied concentrations. As previously mentioned, this could be related to failure resistance and crack propagation. The amount of fibers in the composite and the surface of the fracture plane suggest the presence of exfoliated structures.

6.6 Structure and morphology – SAXS

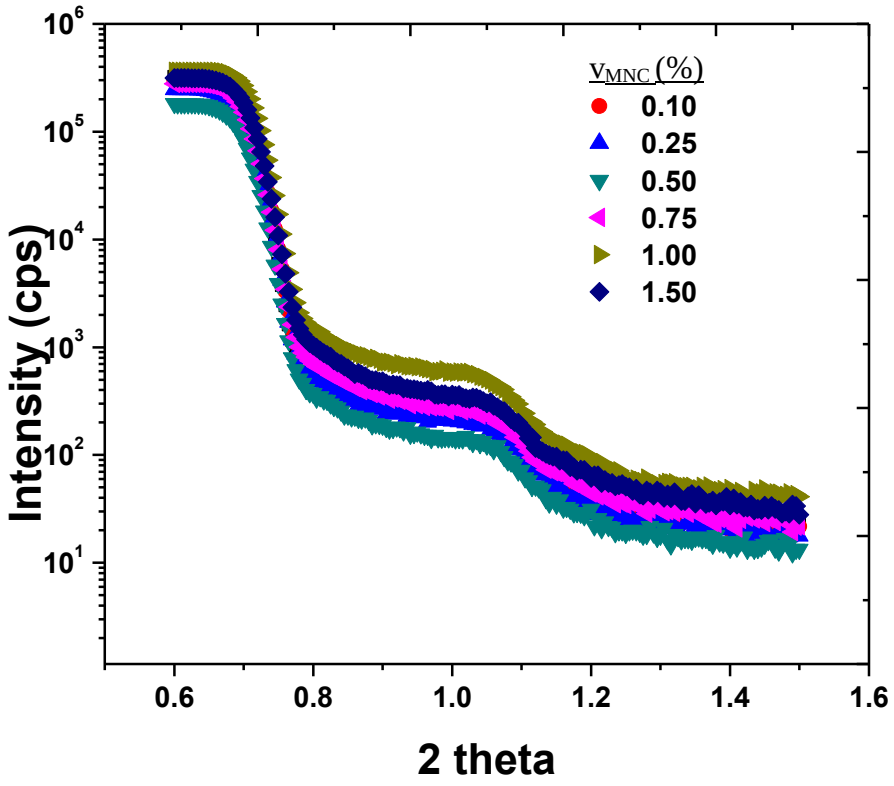

Figure 6.5. Effect of MNC particles on the SAXS patterns of PHBA/PET comoposites.

SAXS analysis shows a spread range of intensities for the different MNC concentrations but no difference in the characteristic peak or angle position, which

means that liquid crystalline phase, is not affected. Also a more flattened peak is observed, if compared with the other particles SAXS, which may be related to the presence of different sized crystal domains.

6.7 Conclusion

Addition of MNC particles significantly enhances composite thermal properties, almost systematically with the amount of particle loading. All degradation temperatures studied were increased by at least 16 ºC and a significant temperature enhancement was evidenced as T_5 increased by more than 20 ºC. This result is very attractive for applications were components demand a high temperature resistance.

In the case of transition temperatures MNC does not significantly affect the glass temperature. This could be an evidence of an exfoliated particle dispersion induced by its morphology and structural arrangement. The melting point decreased, which is not desirable for thermal applications.

The formation of spherulites is observed in all of the POM micrographs, which is a possible evidence of exfoliated or very well dispersed particles. But no significant difference is observed in the nematic phases as particle concentration changes. While for the SEM micrographs fibrillar structures were observed at the fracture plane which indicates that MNC can enhance composite mechanical properties. Liquid crystalline

phase was not affected by the MNC as no significant difference was found between the neat matrix and the composites but evidence of exfoliated structures was found since the peak intensities varied and peak area was increased at different particle loadings.

MNC could be forming exfoliated structures, which also promote the formation of fibrillated structures. These particles enhance matrix resistance to temperature degradation but causes melting point to be diminished with the increment of particle amount. To conclude, addition of MNC affect liquid crystalline phase as evidenced by the POM and SAXS techniques since a flattered peak is observed, which could be evidence of the formation of different domain sizes.

7. DISCUSSION AND CONCLUSIONS

Films containing different shaped particles (i.e. cylindrical, spherical and platelet) were produced at six different concentrations using a liquid crystalline polymer matrix with the goal of evaluating the effect of particle morphology on the liquid crystal phase. These effects were studied by monitoring the behavior of the composite thermal transitions, liquid crystalline structure and thermal stability. The selection of a liquid crystalline matrix relied on the advantageous properties that these materials may provide due to their anisotropy.

In this work, the effect of particle shape and concentration on thermal transitions and composite thermal stability was studied. As shown in Figure 7.1, no effect of particle shape is observed at the T_g transition with varying concentration since there is no statistical difference. In the case of T_m and T_{IN} no effect was observed as a function of particle loading for the MWCNT, HNC and silica systems. On the other hand for MNC both T_m and T_{IN} were displaced to lower values after reaching a concentration of 0.5 v% and higher, but remained independent of particle concentration after the step-like decrease.

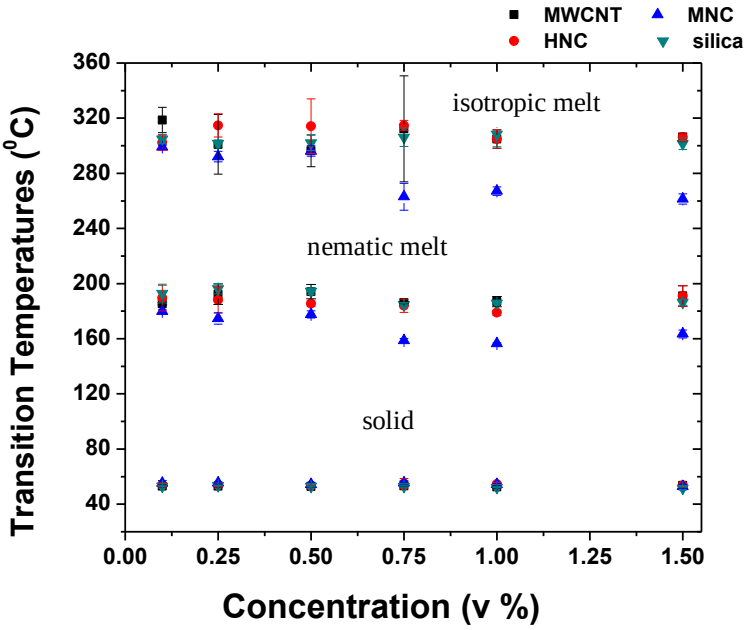

Figure 7.1. Composites Transition Temperatures Phase Diagram.

The temperature range where the liquid crystalline region lies was decreased for the systems (i.e. MWCNT, HNC, MNC and silica) by 31.7 ºC, 14.8 ºC, 38.7 ºC and 32.45 ºC, respectively. These values are the difference between the neat polymer and the average for all systems concentrations, which are summarized in Appendix I.

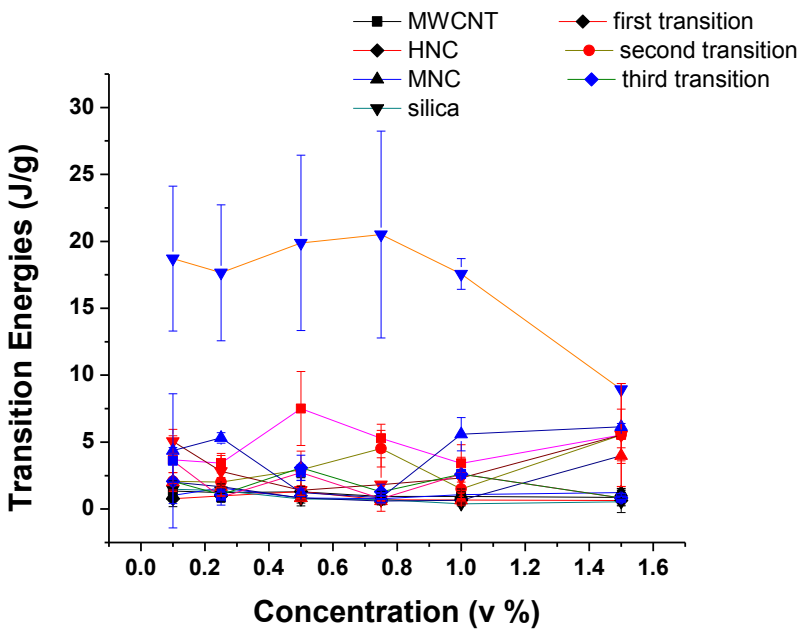

Figure 7.2. Composites Transition Energies Phase Diagram.

Transition energies were collected to see if there was any change in the energy requirement for each phase to be reached. All transition energies (ΔH) remain inside the statistical error, which means that no significant changes on the transition enthalpies can be ensured. Figure 7.2 shows the behavior of all transition energies where it is clearly seen that for the first and second thermal transitions (i.e. glass and melt respectively) all values remain inside the error range despite their individual tendencies of increasing or decreasing. As it can be seen, the isotropic-to-nematic transition for

silica concentrations ranging from 0.1 v% to 1.0 v% had the higher energy values which could be attributed to the greater heat absorption from silica which is then released at this exothermic transition.

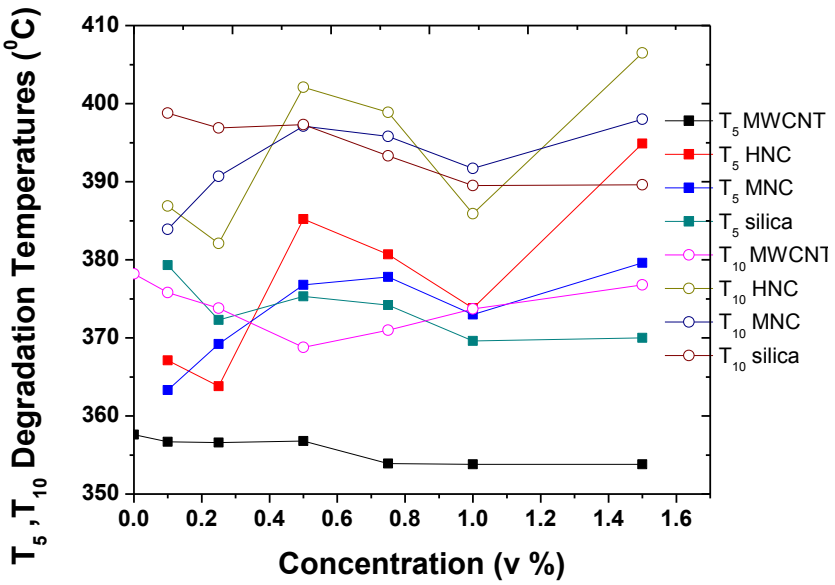

Figure 7.3. Composites Thermal Stability for early degradation.

From the studied systems, MWCNTs showed the less thermal stability enhancement as shown in Figure 7.3 and Figure 7.4. Figure 7.3 shows the thermal stability at 5 and 10 % of weight loss, which in practical terms gives information of how good a material with this composition will be for high temperature applications.

The systems composed by clays and minerals (i.e. HNC, MNC & silica) are the most temperature resistant, which is attributed to the intrinsic properties of these particles and their structural conformation which makes them heat retardant materials.

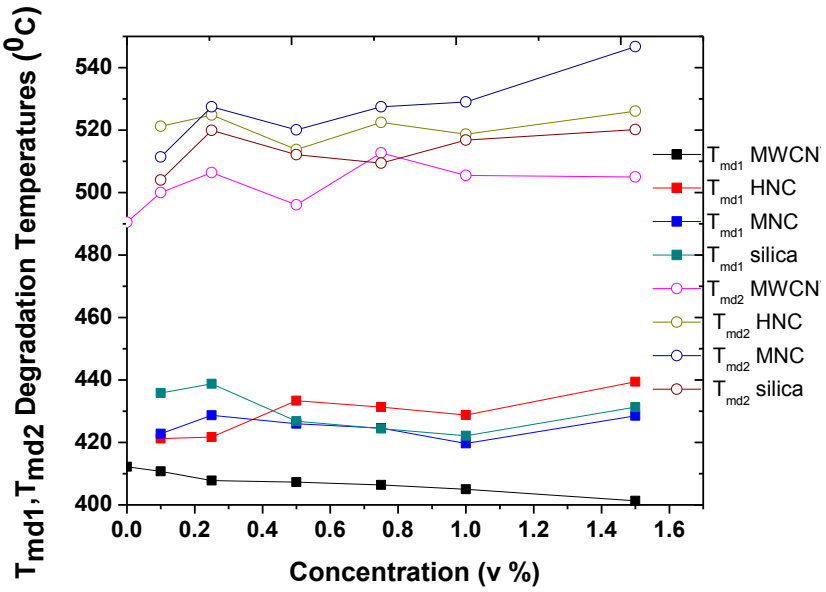

Figure 7.4. Composites Thermal Stability for Major Degradation.

Composites thermal stability or temperature resistance for the particle-matrix interactions is summarized in Figure 7.4, since this figure shows the behavior of all systems at the two major degradation stages and how the interactions of these particles affect the characteristic degradations of the co-polymer components. The same particle

order in terms of thermal stability is maintained as HNC again has the higher temperature trend for the first degradation stage, which corresponds to the degradation of the flexible (PET) domains of the co-polymer. Temperature enhancement could be attributed to the formation of hydrogen bonds with PHBA/PET through the hydroxides present in MNC and HNC structures. Also the gallery arrangement in clays is a factor that helps in composite thermal stability since there will by a high surface area for the energy to be dissipated or retarded. In the case of MWCNT, the first stage is not favored since it has a slight decrease as particle loading increases, which could be due to the increment in rigidity on the flexible side of the co-polymer as part of the increment in MWCNT concentration. This increment in concentration can make the PET molecules more confined, restricting its movement as temperature rises in order to find a better conformation which will translate in the faster degradation of this domain.

For the second degradation stage MNC particles showed the better temperature resistance. In this case MWCNT system show a slight increment in their temperature resistance, this could be related to the migration of MWCNT to the acidic region of the co-polymer (HBA rich domains) since MWCNT like acidic regions. In the case of silica, thermal stability could be related to the bond formation between silica and CH_3 groups.

In the case of liquid crystalline structure, no negative effect was found as the characteristic peak was present and unaffected in all SAXS patterns with the difference that for silica and MNC particles a flattened peak was observed. This widening could be related to the presence of larger distribution of crystal domains which will increase the distribution of scattered rays. The SEM results showed that systems containing rod and platellet-like nanoparticles will maintain the fibrillar nature of the matrix while spherical shaped particles will interfere with the formation of fibrillar structures.

Addition of the nanoparticles at the low concentrations studied does not have a significant effect on the thermal transitions since all values remain inside the experimental error, except for medium to high concentrations of MNC. Liquid cristallinity was maintained throughout the whole range of concentrations and particle shapes as evidenced by POM, but the range was reduced. Furthermore, no significant change seems to be promoted on the liquid crystalline structure for rod-like nanoparticles. But large molecules such as that of MNC with irregular shapes as well as particles which does not impart a preferential orientation could extend or disperse throughout domains. While thermal stability was better promoted with clays and silica than with MWCNT. Other properties such as the thermal stability were mainly affected by the intrinsic properties of the particles and not by their shape or concentration. In

conclusion, at these low loadings particle shape does not have a significant effect on the liquid crystalline structure or thermal transitions of our model LC polymer.

APPENDIX I

Summary of thermal propeties:

Material	v%	T_5	T_{10}	T_{md1}	T_{md2}	T_g	T_m	T_{IN}	(T_m-T_g)	$(T_{IN}-T_m)$	ΔH_g	ΔH_m	ΔH_{IN}
neat	0	357.6	378.2	412.2	490.5	52.5	184.2	330	131.7	145.8	1.01	3.54	1.25
MWCNT	0.1	356.7	375.8	410.7	500	53.0	185.3	318.7	132.3	133.4	0.607	3.69	1.20
	0.25	356.6	373.8	407.8	506.4	53.0	192.4	301.0	139.4	108.6	0.515	4.13	0.896
	0.5	356.8	368.8	407.3	496.1	52.8	194.9	296.9	142.1	102	0.589	4.66	2.06
	0.75	353.9	371.0	406.4	512.7	53.2	186.2	293.1	133	106.9	0.564	4.47	1.00
	1.0	353.8	373.7	405.0	505.2	52.2	186.9	304.7	134.7	117.8	0.307	4.55	0.926
	1.5	353.8	376.8	401.3	505.0	53.5	191.0	306.7	137.5	115.7	0.203	5.53	0.714
HNC	0.1	367.1	386.9	421.2	521.2	52.4	184.2	322.0	131.8	137.8	0.767	2.39	1.18
	0.25	363.8	382.1	421.7	524.8	53.8	188.06	314.8	134.26	126.74	0.978	3.21	1.08
	0.5	385.2	402.2	433.4	513.8	53.2	185.5	314.1	132.3	128.6	0.866	4.66	1.05
	0.75	380.7	398.9	431.3	522.5	55.0	184.0	314.7	129	130.7	0.723	4.85	0.883
	1.0	373.8	385.9	428.8	518.7	54.5	178.9	311.5	124.4	132.6	0.945	5.99	0.971
	1.5	394.9	406.5	439.4	526.1	59.8	182.7	312.3	122.9	129.6	0.800	6.42	0.961
silica	0.1	379.3	398.8	435.8	504.0	53.0	182.4	302.3	129.4	119.9	1.17	2.40	11.12
	0.25	372.3	396.5	438.8	519.9	53.5	186.8	301.8	133.3	115	1.29	1.78	19.12
	0.5	375.3	397.3	426.8	512.1	52.5	198.2	300.9	145.7	102.7	0.447	4.35	12.22
	0.75	374.2	393.3	424.4	509.4	52.4	192.4	304.1	140	111.7	0.590	3.59	12.89
	1.0	369.6	389.5	422.1	516.8	54.8	193.0	307.0	138.2	114	0.311	2.89	12.74
	1.5	370	389.6	431.3	520.2	51.3	185.2	302.0	133.9	116.8	0.495	1.94	12.48
MNC	0.1	363.3	383.9	422.8	511.4	53.5	178.8	297.6	125.3	118.8	0.929	2.79	4.35
	0.25	369.2	390.7	428.7	527.5	54.9	171.4	287.8	116.5	116.4	1.60	1.21	5.49
	0.5	376.8	397.1	426.0	520.1	53.0	177.7	291.9	124.7	114.2	0.656	10.7	0.927
	0.75	377.8	395.8	424.6	527.5	53.7	158.6	252.0	104.9	93.4	0.792	0.564	0.866
	1.0	373.0	391.7	419.7	529.0	53.6	156.1	264.1	102.5	108	1.17	0.623	4.40
	1.5	379.6	398.0	428.5	546.7	54.6	166.3	258.3	111.7	92	1.24	4.66	6.33

REFERENCES

1. Gupta, R.K., V. Pasanovic-Zujo, and S.N. Bhattacharya, *Shear and extensional of EVA/layered silicate-nanocomposites.* Journal of Non-Newtonian Fluid Mechanics, 2005. **128**: p. 116-125.
2. Wang, D.C., G.C. Chang, and Y. Chen, *Preparation and thermal stability of boron-containing phenolic resin/clay nanocomposites.* Polymer Degradation and Stability, 2008. **93**: p. 125-133.
3. Boccaccini, A.R. and V. Maquet, *Bioresorbable and bioactive polymer/Bioglass composites with tailored pore structure for tissue engineering applications.* Composites Science and Technology, 2003. **63**(16): p. 2417-2429.
4. Kumar, R. and A.I. Isayev, *Thermotropic LCP/CNF nanocomposites prepared with aid of ultrasonic waves.* Polymer, 2010. **51**: p. 3503-3511.
5. http://www.britanica.com/EBchecked/topic/72869/bone/41882/Chemical-composition-and-physical-properties. [cited May 23, 2010].
6. Onder, A., *FIRST FAILURE PRESSURE OF COMPOSITE PRESSURE VESSELS*, in *Mechanical Engineering*. 2007, Dokuz Eylül University. p. 129.
7. Gibson, R.F., *A review of recent research on mechanics of multifunctional composite materials and structures.* Composite Structures, 2010.
8. Koo, J.H., *Polymer nanocomposites: Processing, Characterization and Applications*. Nanoscience and technology Series, ed. McGraw-Hill.
9. Colonna, M., et al., *Nanocomposite of Montmorillonite with telechelic sulfonated poly(butylene terephthalate): effect of ionic groups on clay dispersion, mechanical and thermal properties. (Accepted Manuscript).* European Polymer Journal, 2010.
10. Rao, V.V.S. and P.K. Sinha, *Dynamic Response of Multidirectional Composites in Hygrothermal Environments.* Composite Structures, 2004. **64**: p. 329-338.
11. Uddin, M.F. and C.T. Sun, *Strength of unidirectional glass/epoxy composite with silica nanoparticle-enhanced matrix.* Composites Science and Technology, 2008. **68**: p. 1637–1643.
12. Alexandre, M. and P. Dubois, *Polymer-layered silicate nanocomposites: preparation,properties and uses of a new class of materials*, in *Reports: A Review Journal*, M.S.a. Engineering, Editor. 2000, Laboratory of Polymeric and Composite Materials, University of Mons-Hainaut, Belgium: Mons, Belgium. p. 1-63.
13. http://www.azom.com/details.asp?articleid=921. [cited May 23, 2010].

14. Jun Young Kim, D.K.K., Seong Hun Kim, *Effect of modified carbon nanotube on physical properties thermotropic liquid crystal polyester nanocomposites.* European Polymer Journal, 2009. **45**: p. 316-324.
15. Campell, K., D.Q.M. Craig, and T. McNally, *Poly(ethylene glycol) layered silicatenanocomposites for retarded drug release prepared by hot melt extrusion.* International Journal of Pharmaceutics, 2008. **363**: p. 126-131.
16. Shen, H.S., *Nonlinear bending of functionally graded carbon nanotube reinforced composite plates in thermal environments.* Composite Structures, 2009. **91**: p. 9-19.
17. http://composite.about.com/library/PR/2001/blpsu2.htm. [cited May 23, 2010].
18. Choudalakis, G. and A.D. Gotsis, *Permeability of polymer/clay nanocomposites: A review.* European Polymer Journal, 2009. **45**: p. 967–984.
19. Gilman, J.W. and T. Kashiwagi, *Nanocomposites: A revolutionary new flame retardant approach*, in *42nd International SAMPE Symposium*, P.L. Joseph D. Lichtenhan, Editor. 1997.
20. Herrera-Alonso, J.M., et al., *Transport properties in polyurethane/clay nanocomposites as barrier materials: Effect of processing conditions.* Journal of Membrane Science, 2009. **337**: p. 208-214.
21. Zhao, C., et al., *Mechanical, thermal and flammability properties of polyethylene/clay nanocomposites.* Polymer Degradation and Stability, 2005. **87**: p. 183-189.
22. Chandra, A., et al., *Study of utilizing thin polymer surface coating on the nanoparticles for melt compounding of polycarbonate/alumina nanocomposites and their optical properties.* Composites Science and Technology 2008. **68**: p. 768-776.
23. Han, K. and M. Yu, *Study of the preparation and properties of UV- blocking fabrics of a PET/TiO2 nanocomposites prepared by in-situ polycondensation.* Journal of Applied Polymer Science, 2006. **100**: p. 1588-1593.
24. Garcıa-Lopez, D., et al., *Polypropylene–clay nanocomposites: effect of compatibilizing agents on clay dispersion.* European Polymer Journal, 2003. **39**: p. 945-950.
25. Mai, Y.-W. and Z.Z. Yu, eds. *Polymer nanocomposites*. 2006, Published in North America by CRC Press LLC, 6000 Broken Sound Parkway, NW, Suite 300, Boca Raton, FL 33487, USA: Cambridge England.
26. Collings, P.J., *Liquid Crystals: Nature's delicate phase of matter*, ed. P.S. Library. 1990, Princeton, New Jersey: Princeton University Press. 221.
27. Singh, S., *Liquid Crystals: Fundamentals*. 2002, London: World Scientific Publishing Co. Pte. Ltd. 549.

28. Bushby, R.J. and O.R. Lozman, *Discotic liquid crystals 25 years on.* Current Opinion in Colloid & Interface Science, 2002. **7**: p. 343-354.
29. Dierking, I., *Crystallisation of a bent-core liquid crystal mesogen.* Physica B, 2001. **304**: p. 51–59.
30. So, B.-K., et al., *Novel bent-shaped liquid crystalline compounds: III. Synthesis of Schiff base liquid crystal dimers.* Dyes and Pigments, 2007. **75**: p. 619-623.
31. Dong, R.Y., et al., *High nematic ordering in a bent-core smectogen showing a biaxial nematic phase: A 13C NMR study.* Chemical Physics Letters, 2007. **448**: p. 54-60.
32. Francesco Paolo La Mantia, *Thermotropic Liquid Crystal Polymer Blends*. 1993, Lancaster Pensylvania: Technomic Publishing Company, Inc. 177.
33. Wang, X.-J. and Q.-F. Zhou, *Liquid Crystalline Polymers*. 2004, Danvers, MA: World Scientific Publishing Co. Pte. Ltd. 389.
34. Donald, A., A. Windle, and S. Hanna, *Liquid Crystalline Polymers*. 2005: Cambridge University Press. 574.
35. Sun, T., et al., *Phase transitions of poly(ethylene terephtalate-co-p-hydroxybenzoic acid) liquid crystal by dynamic mechanical analysis.* Polymer, 1988. **30**: p. 1257-1261.
36. Yoon, D.Y., et al., *High-Temperatures Structures of Poly(p-hydroxybenzoic acid-co-ethylene terephthalate).* Macromolecules, 1989. **23**: p. 1793-1799.
37. Larson, R.G., *The Structure and Rheology of Complex Fluids*. Topics in Chemical Engineering, ed. N.C.S.U. Keith E. Gubbins. 1999, New York-Oxford: Oxford university Press.
38. http://www.google.com/imgres?imgurl=http://www.rsc.org/ejga/CC/2002/b209193c-ga.gif&imgrefurl=http://www.rsc.org/publishing/journals/CC/article.asp%3Fdoi%3Db209193c&usg=__5_2xrtYwXDZAmAiVWQR1UlvDRBM=&h=206&w=367&sz=26&hl=en&start=140&tbnid=mbL3LPTA7QB2XM:&tbnh=115&tbnw=204&prev=/images%3Fq%3Dmain%2Bchain%2Bpolymer%2Bimages%26um%3D1%26hl%3Den%26sa%3DX%26biw%3D1280%26bih%3D683%26tbs%3Disch:10,4520&um=1&itbs=1&iact=hc&vpx=522&vpy=347&dur=10012&hovh=164&hovw=293&tx=137&ty=47&ei=jeReTJXWCoL48Abd4fCUBw&oei=A-ReTKurG4K88gbgxL22DQ&esq=12&page=9&ndsp=18&ved=1t:429,r:8,s:140&biw=1280&bih=683. [cited 2010 August 6].

39. Karim, M.A., et al., *Development of liquid crystal embedded in polymer electrolytes composed of click polymers for dye-sensitized solar cell applications.* Dyes and Pigments, 2010. **86**: p. 259-265.
40. Athene Donald, A.W.a.S.H., *Liquid Crystalline Polymers*. 2005: Cambridge University Press. 574.
41. Ramamoorthy, A., *Thermotropic Liquid Crystals*. 2007, Dordrecht, The Netherlands: Springer. 272.
42. Lin, J.-S., *Effect of surface modification by bromination on Kevlar fibre-epoxy adhesion.* European Polymer Journal, 2002. **38**: p. 2002.
43. Dang, T.D., et al., *Polybenzobisthiazoles with crosslinking sites for improved fibre axial compressive strength.* Polymer, 1997. **38**(3): p. 621-629.
44. Samuel, P., et al., *New opportunities for research in coal derived chemicals.* Journal of Scientific and Industrial research, 2008. **67**: p. 1051-1058.
45. Saikrasun, S. and O. Wongkalasin, *Thermal decomposition kinetics of thermotropic liquid crystalline p-hydroxy benzoic acid/poly(ethylene terephthalate) copolyester.* Polymer Degradation and Stability, 2005. **88**: p. 300-308.
46. Zülle, B., et al., *Processing, morphology and properties of a thermotropic liquid crystalline polymer.* Polymer, 1993. **34**(17): p. 3628-3637.
47. Zhang, H., G.R. Davies, and I.M. Ward, *Mechanical properties of thermotropic liquid crystalline polyesters and polyamides.* Polymer, 1992. Polymer(13): p. 2651-2658.
48. Kim, J.Y., D.K. Kim, and S.H. Kim, *Effect of modified carbon nanotube on physical properties thermotropic liquid crystal polyester nanocomposites.* European Polymer Journal, 2009. **45**: p. 316-324.
49. McLeod, M.A. and D.G. Baird, *The crystallization behavior of blends of thermotropic liquid crystalline polymers.* Polymer, 1999. **40**: p. 3743–3752.
50. Gopakumar, T.G., et al., *In situ compatibilisation of poly(phenylene sulphide)/wholly aromatic thermotropic liquid crystalline polymer blends by reactive extrusion: morphology, thermal and mechanical properties.* Polymer, 1999. **34**(17): p. 357-364.
51. Xue, Y. and M. Hara, *Novel blends made of ionic naphthalene thermotropic polymer and poly(ethylene terephthalate).* Polymer, 2006. **47**: p. 6710-6717.
52. Yu, R., et al., *Extensional viscosity of a thermotropic liquid crystalline polymer measured by thread disintegration method.* Polymer testing, 2005. **24**: p. 513-518.
53. Lee, S., et al., *Effect of carbon nanofibers on the anisotropy of an aromatic thermotropic liquid crystalline polymer.* Polymer, 2005. **46**: p. 2663-2667.

54. Souza, J.P.d. and D.G. Baird, *In situ composites based on blends of a poly(ether imide) and thermotropic liquid crystalline polymers under injection moulding conditions.* Polymer, 1996. **37**(10): p. 1985-1997.
55. Baird, D.G. and D.I. Collias, *Extruders*, in *Polymer processing: Principles and design*
1998, John Wiley & Sons, Inc.: Blacksburg, VA. p. 213-246.
56. Cartier, H. and G. Hua-Hu, *A novel reactive extrusion process for compatibilizing immicible polymer blends.* Polymer, 2001. **42**: p. 8807-8816.
57. Kartika, I.A., P.Y. Pontalier, and L. Rigal, *Oil extraction of oleic sunflower seeds by twin screw extruder:*
influence of screw configuration and operating conditions. Industrial crops and products: an international journal, 2005. **22**: p. 207-222.
58. Zuilichem, D.J.v., et al., *Mixing effects of constituting elements of mixing screws in single and twin screw extruders.* Powder Technology, 1999. **106**: p. 147–159.
59. Baird, D.G. and D.I. Collias, *Importance of process design*, in *Polymer processing: Principles and design*. 1998, John Wiley & Sons, Inc.: Blacksburg. VA. p. 1-8.
60. Hong, Y., et al., *Film blowing of linear low-density polyethylene blended with a novel hyperbranched polymer processing aid.* Polymer, 2000(41): p. 7705–7713.
61. López, J., et al., *Analysis weld seam weak in blow molding large parts made of commodity plastics.* Engineering Failure Analysis, 2009. **16**: p. 856–862.
62. Chen, S.-C., et al., *Study on the thermoforming of PC films used for in-mold decoration.* International Communications in Heat and Mass Transfer, 2008. **35**: p. 967-973.
63. http://www.plasticstech.info/processes/extrusion/blown-film-extrusion/blown-film-extrusion.gif.[cited August 20, 2010].
64. Liang, J.-Z., *Characteristics of melt shear viscosity during extrusion of*
polymers. Polymer testing, 2002. **2002**: p. 307-311.
65. Xu, B., et al., *Calculating barrier properties of polymer/clay nanocomposites: Effects of clay layers.* Polymer, 2006. **47**: p. 2904-2910.
66. Campbell, K., D.Q.M. Craig, and T. McNally, *Poly(ethylene glycol) layered silicate nanocomposites for retarded drug release prepeared by hot-melt extrusion.* International Journal of Pharmaceutics, 2008. **363**: p. 126 - 131.
67. Gabriele, D., S. Curcio, and B.d. Cindio, *Optimal design of single-screw extruder for liquorice candy*
production: a rheology based approach. Journal of food and engineering, 2001. **48**: p. 33-44.

68. Yeh, A.-I. and Y.-M. Jaw, *Predicting residence time distributions in a single screw extruder from*
operating conditions. Journal of food and engineering, 1999. **39**: p. 81-89.
69. Russo, G.M., et al., *Rheological and mechanical properties of nylon 6 nanocomposites*
submitted to reprocessing with single and twin screw extruders. Polymer Degradation and Stability, 2007. **92**: p. 1925-1933.
70. Rauwendaal, C., *Different types of extruders*, in *Polymer extrusion*. 2001, HANSER: Menlo Park, CA. p. 11-33.
71. Chokshi, R. and H. Zia. *Hot-Melt Extrusion Technique: A Review.* http://www.slscrewbarrel.com/news/?nid=33]. [cited July 17, 2011].
72. Hertel, D., *Flow of polyethylene melts within and into rectangular ducts investigated by laser - Doppler velocimetry*. 2008, Universität Erlangen-Nürnberg: Erlangen-Nürnberg.
73. Shenoy, A.V., *Rheology of filled polymer systems*. 1999, Pune, INdia.
74. Kim, J.Y., D.K. Kim, and S.H. Kim, *Effect of modified carbon nanotube on physical properties of thermotropic liquid crystal polyester nanocomposites.* European Polymer Journal, 2009. **45**: p. 316-324.
75. Joseph, R., et al., *Effect of hydroxyapatite morphology/surface area on the rheology and processability of filled polyethylene composites.* Biomaterials, 2002. **23**: p. 4295-4302.
76. Dangtungee, R. and P. Supaphol, *Melt rheology and extrudate swell of sodium chloride-filled low-density polyethylene: Effects of content and size of salt particles.* Polymer Testing, 2010. **29**: p. 188-195.
77. Dungtangee, R. and P. Supaphol, *Melt rheology and extrudate swell of titanium (IV) oxide nanoparticle-filled isotactic polypropylene: Effect of content and surface characteristics.* Polymer Testing, 2008. **27**: p. 951-956.
78. Leblanc, J.L., *Rubber-filler interactions and rheological properties in filled compounds.* Progress in polymer science, 2002. **27**: p. 627-687.
79. Kasaliwal, G.R., et al., *Analysis of agglomerate dispersion mechanisms of multiwalled carbon nanotubes during melt mixing in polycarbonate.* Polymer, 2010. **51**: p. 2708e2720.
80. Xie, X.-L., Y.-W. Mai, and X.-P. Zhou, *Dispersion and alignment of carbon nanotubes in polymer matrix: A review.* Materials Science and Engineering, 2005. **R 49**: p. 89–112.
81. Causina, V., et al., *Assessing organo-clay dispersion in polymer layered silicate nanocomposites: A SAXS approach.* Polymer, 2005. **46**: p. 9533–9537.
82. Manitiu, M., et al., *Role of polymer-clay interactions and nano-clay dispersion on the viscoelastic response of supercritical CO2 dispersed*

polyvinylmethylether (PVME)-Clay nanocomposites. Polymer, 2009. **50**(15): p. 3786-3796.

83. Huang, W. and C.D. Han, *Dispersion characteristics and rheology og organoclay nanocomposites based on a segmented main-chain liquid-crystalline polymer having side-chain azopyridine with flexible spacer*. 2006, ELSEVIER. p. 4400-4410.
84. Incarnato, L., O. Motta, and D. Acierno, *Thermal behavior of the PET/Rodrun 3000 system.* Polymer, 1997. **39**: p. 5085-5095.
85. Brostow, W., J.M. Hess, and B.L. Lopez, *Phase Structures and Phase Diagrams in Polymer Liquid-Crystal Systems: Copolymers of Poly(ethy1ene terephthalate) and p-Hydroxybenzoic acid.* Macromolecules, 1994. **27**: p. 2262-2269.
86. Vallejo, F.J., J.I. Eguiazábal, and J. Nazábal, *Blends of a thermotropic copolyester and a thermotropic copoly(ester-amide): structure and mechanical properties.* Polymer, 2001. **42**: p. 9593-9599.
87. Saengsuwana, S., et al., *Thermotropic liquid crystalline polymer (Rodrun LC5000)/polypropylene in situ composite films: rheology, morphology, molecular orientation and tensile properties.* Polymer, 2003. **44**: p. 3407–3415.
88. *http://cheaptubes.com/coohfunctionalizedcnts.htm#_COOH_Functionalized_Nanotubes_8nm_Specifications*.
89. Baumeister, E., S. Klaeger, and A. Kaldos, *Lightweight, hollow-sphere-composite (HSC) materials for mechanical engineering applications.* Journal of Materials Processing Technology, 2004. **155–156**: p. 1839-1846.
90. Larsson, F. and L. Svensson, *Carbon, polyethylene and PBO hybrid fibre composites for structural lightweight armour* Composites Part A: Applied Science and Manufacturing. **33**(2): p. 221-231.
91. Adell, J.M., et al., *Structural modifications and fibre processing of hydroxy-functionalised mesogenic polyazomethines.* Polymer, 2003. **44**: p. 7829–7841.
92. Kiliaris, P. and C.D. Papaspyrides, *Polymer/layered silicate (clay) nanocomposites: An overview of flame retardancy*
Progress in Polymer Science, 2010. **35**: p. 902–958.
93. Carter, N., et al., *High temperature non-aqueous dispersion polymerisation of aromatic main chain liquid crystal polymers using organo-clay stabilisation.* Polymer 1999. **40**: p. 7233–7241.
94. Sugiyama, H., et al., *Structural characteristics, rheological properties, extrusion, and melt spining of 60/40 Poly(Hydroxybenzoic acid-coethylene terephthalate) (PHB/PET).* Applied Polymer Science, 1985. **30**: p. 2329-2341.
95. Menczel, J. and B. Wunderlich, Polymer Science, 1980. **18**.

96. Vaia, R.A. and E.P. Giannelis, Polymer, 2001. **42**: p. 1281-1285.
97. Pavlidou, S. and C.D. Papaspyrides, Progress in Polymer Science, 2008. **33**: p. 1119–1198.
98. Azeredo, H.M.C.d., Food Research International, 2009. **42**: p. 1240–1253.
99. Ray, S.S. and M. Okamoto, Progress in Polymer Science, 2003. **28**: p. 1539–1641.
100. Bistricˇic´, L., et al., European Polymer Journal, 2010. **46**: p. 1975–1987.
101. Liu, Y.-L., et al., Polymer, 2003. **44**: p. 5159–5167.
102. Lee, M.W., et al., Composites Science and Technology, 2003. **63**: p. 1921–1929.
103. Pfaendner, R., Polymer Degradation and Stability, 2010. **95**: p. 369e373.
104. Qin, Y., et al., Polymer, 1993. **34**: p. 3597–604.
105. Soundararajah, Q.Y., B.S.B. Karunaratne, and R.M.G. Rajapakse, *Montmorillonite polyaniline nanocomposites: Preparation, characterization and investigation of mechanical properties.* Materials Chemistry and Physics, 2009. **113**: p. 850-855.
106. Golebiewski, J., et al., *Low density polyethylene–montmorillonite nanocomposites for film blowing.* European Polymer Journal, 2008. **44**: p. 270–286.